BAG3 regulation of Rab35 mediates the ESCRT/endolysosome pathway and tau clearance

Heng Lin, Maoping Tang[$], Changyi Ji[^], Peter Girardi, Gregor Cvetojevic, Yunpo Chen,

Gail V. W. Johnson[*]

Department of Anesthesiology and Perioperative Medicine , University of Rochester, 601 Elmwood Ave, Box 604, Rochester, NY 14642 USA

[$]Current address: School of Pharmacy, Shanghai Jiao Tong University, Shanghai, Minhang District, 200240 China.

[^]Current address: New York University School of Medicine, Department of Neuroscience and Physiology, Neuroscience Institute, 11th floor 1123F, 435 East 30th St., New York, NY 10016 USA

* Correspondence should be addressed to:

Gail V.W. Johnson, PhD
Department of Anesthesiology and Perioperative Medicine
University of Rochester
601 Elmwood Ave, Box 604
Rochester, NY 14642
gail_johnsonvoll@urmc.rochester.edu
+1-585-276-3740 (voice)

Abstract

The decline in proteostasis during aging is a major contributing factor to increased susceptibility to neurodegenerative diseases such as Alzheimer's disease. Although dysfunction of the autophagy pathway is likely one of the contributors, emerging studies implicate that impairment of the endosome-lysosome pathway is also a significant factor in the pathogenesis of these diseases. Our lab was the first to demonstrate that BAG3 facilitates phosphorylated tau clearance through autophagy. However, we did not fully define the mechanisms by which BAG3 regulates endogenous tau proteostasis. Here, we applied mass spectrometric analyses and found a major group of neuronal BAG3 interactors are in the endocytic pathway. Among them were key regulators of small GTPases. Excitingly one of these was the Rab35 GTPase activating protein, TBC1D10B. Our data demonstrate that a BAG3-HSP70-TBC1D10B complex attenuates the ability of TBC1D10B to inactivate Rab35. Thus BAG3, through its interaction with TBC1D10B supports the activation of Rab35 and recruitment of Hrs, which initiates ESCRT-mediated endosomal tau clearance. Further, intrahippocampal expression of BAG3 in P301S mice increased the co-localization of phospho-tau with the ESCRT III protein CHMP2B and reduced the levels of the mutant human tau. Overall, our data provide evidence of a novel BAG3-TBC1D10B-Rab35 regulatory axis in modulating vacuolar dependent protein degradation machinery through ESCRT. These findings expand our understanding of the role of BAG3 in neuronal proteostasis, and how dysregulation could contribute to the pathogenesis of Alzheimer's disease, as well as other neurodegenerative diseases.

Keywords: Tau, BAG3, ESCRT, Hrs, Rab35, TBC1D10B

Introduction

Maintaining proteostasis is vital for neuronal function and healthy aging. A critical aspect of proteostasis is an efficient system that recognizes damaged or unnecessary proteins and clears them from the cell. Disruption of proteome homeostasis is likely a significant contributing factor to the pathogenesis of neurodegenerative diseases that are characterized by the accumulation of aggregation prone proteins, such as Alzheimer's disease (AD)[29,49]. One of the defining hallmarks of AD is the presence of intraneuronal aggregates of phosphorylated tau [54]. The accumulation of tau, particularly in an oligomeric state, contributes to AD pathogenesis [14]. There is increasing evidence that compromised degradative mechanisms, and in particular lysosome dysfunction, likely contribute to the accumulation of toxic tau species, as well as other disease relevant proteins [58,37].

Degradative pathways that direct cargos to the lysosome include autophagosome-lysosome and endosome-lysosome pathways, both of which are highly regulated, vacuolar-based degradative systems. Although dysfunction of the autophagy pathway is likely one of the contributors to neurodegenerative proteopathies such as AD and Parkinson's disease [52,11], it is clear that impairment of the endosome-lysosome pathway is also a significant contributor to the pathogenesis of these diseases [75,61]. The endosome-lysosome pathway is an important protein clearance mechanism that directs the engulfment of protein cargo and trafficking to the lysosome for degradation. A key to this process is the endosomal sorting complex required for transport (ESCRT) machinery, which mediates multivesicular body (MVB) formation and fusion with the lysosome [55]. Additionally, deficits in ESCRT and the endosome-lysosome pathway have been observed in AD and other neurodegenerative diseases [32]. For example, enlargement of the early endosome compartment and increased endosome/ysosome pH have been considered as the some of the earliest pathological changes in AD [10]. Further, studies in cell models have shown that compromised ESCRT leads to endolysosomal escape of tau seeds and propagation of tau aggregation [13], and mutation of the ESCRT III protein CHMP2b causes frontotemporal dementia [67]. Given that defects in the endosome-lysosome pathway likely contribute to the pathogenesis of neurodegenerative diseases, it is of critical importance to understand the regulation of this pathway.

Bcl-2-associated anthogene 3 (BAG3) is a stress-induced, multi-domain protein that plays a critical role in maintaining proteostasis, and thus neuronal health [5,69,82,12]. As a stress-induced protein, BAG3 protein levels increase during ageing [71]. Interestingly, BAG3 is expressed at higher levels in neurons that are resistant to tau pathology compared to those that are susceptible

[23], and recent data suggest that BAG3 levels are lower in AD brain compared to aged-matched controls [82]. BAG3 has been shown to promote the clearance of tau [51] and other disease-relevant aggregation prone proteins such as α-synuclein [8], mutant SOD1, and mutant huntingtin [69]. These findings point to the importance of BAG3 in maintaining neuronal homeostasis, and this supposition is largely due to its ability to facilitate autophagy [5]. Nonetheless, the specific molecular mechanisms by which BAG3 regulates autophagy in neurons have not been unequivocally elucidated and it is becoming apparent that this is likely not the only degradative pathway regulated by BAG3.

Given the importance of BAG3 in maintaining the neuronal proteome, we focused our studies on defining the molecular events regulated by BAG3. Therefore, we carried out an unbiased proteomic screen of BAG3 interactors in neurons by using mass spectrometric analysis of proteins that co-immunoprecipitated with endogenous BAG3. Interestingly, KEGG analysis of the BAG3 associated proteins revealed that the top pathway was the endocytosis pathway. These findings further indicate the potential role of BAG3 in regulating protein homeostasis through modulating the endosomal-lysosome pathway. Of particular interest was the fact that several of the proteins were regulators of small GTPases, and most excitingly we found that the primary GTPase-activating protein (GAP) for Rab35, TBC1D10B((Tre-2/USP6, BUB2, Cdc16) Domain Family 10B), [31] is a bona fide BAG3 interactor. Rab35, which localized to endosomes and the plasma membrane, is involved in vacuole and protein trafficking, synapse vesicle turnover, and protein clearance [45,57,65]. Further, a recent study showed activated Rab35 recruits Hrs/ESCRT-0, and traffics tau as a cargo, to the endosome [72]. These finding suggested that Rab35 plays a central role in the clearance of tau through the ESCRT-mediated endosome-lysosome pathway. Therefore, it is of great importance to understand the regulation of Rab35 activity.

In the present study, we demonstrate that the binding of TBC1D10B by BAG3 inhibits its ability to inactivate Rab35, which in turn keeps Rab35 in a GTP bound, activated state. BAG3 not only promotes the activation of Rab35 and recruitment ESCRT-0/Hrs, but also increase the mobility of Hrs. Furthermore, BAG3 promotes the association of Hrs with tau, and increases phosphorylated tau sorting into MVBs in vivo. Intrahippocampal delivery of BAG3 in P301S tau (PS19 line) mice significantly decreased tau levels, increased the co-localization of phospho-tau with the ESCRT-III protein CHMP2b and increased the density of neurites. Our findings define a new role of BAG3 in regulating vacuolar dependent protein degradation machinery through the TBC1D10B-Rab35-Hrs axis.

Materials and Methods

Reagents

Constructs: lentiviral vectors: shBAG3 (5'-AAGGTTCAGACCATCTTGGAA-3') and BAG3-scrRNA (5'-CAGTCGCGTTTGCGACTGG-3') in FG12 (with an H1 promoter) [51], or pHUUG with a U6 promoter (a generous gift of from Dr. C.Pröschel, University of Rochester) with and without GFP were used. shTBC1D10B (5'-GCTGTCTTAATTTGCCTTTGG-3') and shRab35 (5'-CGATTGTGGTGATGTAGCTG-3' targeting the ORF region and 5'-ATTTGTTAAGAGAATGCTCC-3' targeting the 3'UTR region) were prepared in pHUUG. pcDNA3 TBC1D10B (NM_015527.3 (ORF sequence) in pcDNA3.1+/C-(K)-DYK (FLAG tagged)) was prepared by and purchased from Genscript (Genscript, NJ). Myc-Rab35 (plasmid#47433), Myc-Rab35 Q67L (plasmid #47434), eGFP-Rab35 (plasmid #49552), and pCS2 Hrs-RFP (plasmid #29685) were from Addgene. BAG3, WAWA BAG3 [40] (with W to A substitutions at positions 26 and 49), and L462P BAG3 in pcDNA (generous gifts from Dr. J. Höfeld, University of Bonn) were used as templates to clone into the lentiviral pCDH backbone (System Biosciences CD516-B2, CA) using Gibson assembly (New England Biolabs, #2611, MA). pCDH-GPG BAG3 was generated by mutation of the two IPV domains of BAG3 in pcDNA to GPG (with IPV to GPG substitution at position 95~97 and 207~209) and cloning into the pCDH backbone. pCDH-T4 tau-T2A-RFP was generated by cloning T4 tau (0N4R) from T4 tau-pcDNA3.1 [18] using Gibson assembly into the lentiviral pCDH backbone, replacing the Puromycin resistant gene. pGEX-RBD35 was generated by cloning the Rab35-binding region of RUSC2 (RUN and SH3 domain-containing 2; amino acid residues 982–1,199) from cDNA derived from mouse brain into pGEX-6P-2 (#GE28-9546-50, Millipore Sigma) at the BamH1 and Not1 sites. Lentiviral packaging vectors psPAX2 (#12260) and VSV-G (#12259) were from Addgene. AAV control virus (AAV9-SYN1-eGFP) and AAV BAG3 overexpression virus (AAV9-SYN1-GFP-T2A-BAG3 [with an N terminal FLAG-Myc tag]) were purchased from Vector Biolabs (Vector Biolabs, PA).

Antibodies: rabbit antibodies include: BAG3 (Proteintech, 10599-1-AP), TBC1D10B (Invitrogen, PA5-61832), V5 Tag (Cell Signaling Technology, #13202), Rab35 (Proteintech, 11329-2-AP), PSD95 (Cell Signaling Technology, #3450S), Hrs (Cell Signaling Technology, #15087), tau (Dako, A0024), phospho-Tau (Thr231)(AT180 Thermo Fisher OPA-03156), CHMP2B (Proteintech, 12527-I-AP), Normal Rabbit IgG (EMD Millipore 12-370). Mouse antibodies include: Hrs (Santa Cruz, sc-271455), Myc Tag (Cell Signaling Technology, #2276), FLAG Tag (Cell Signaling Technology, 8146), MAP2 (AP14, a gift from Dr. L.I. Binder [7,60]), clathrin (Santa Cruz, sc-271178), MAP6 (Biolegend, 824701), MC1 (a gift from Dr. P. Davies) , 5A6 (DSHB, Univ. Iowa),

HT7 (ThermoFisher, MN1000B), tau5 (a gift from Dr L.I. Binder [7,60]), T22 (Millipore Sigma, ABN454), phospho-Tau (Ser262) (12E8, a gift from Dr. P. Seubert), phospho-Tau (Ser396/404) (PHF1, a gift from Dr. P. Davies), GAPDH (Invitrogen, AM4300), Normal mouse IgG (EMD Millipore 12-371). Secondary antibodies include Alexa Fluor 594 donkey-anti-rabbit, Alexa Fluor 594 donkey-anti-mouse, Alexa Fluor 488 donkey-anti-mouse, Alexa Fluor 488 donkey-anti-rabbit, and Alexa Fluor 647 donkey-anti-mouse (Thermo Fisher Scientific). Conformation specific mouse anti-rabbit IgG (Cell Signaling Technology, #5127S). Anti-rabbit IgG HRP-conjugated Antibody (Bio-rad 5196-2504), Anti-mouse IgG HRP-conjugated Antibody (Bio-rad 5178-2504).

Animals

All mice and rats were maintained on a 12 h light/dark cycle with food and water available ad libitum. All procedures were approved by University Committee on Animal Research of the University of Rochester. Male P301S mice (PS19 line) were purchased from Jackson laboratories (Stock # 008169). There were 4-5 animals in each group for all quantitative analyses. All procedures were approved and performed in compliance with the University of Rochester guidelines for the care and use of laboratory animals.

To prepare samples for analyses, mice were deeply anesthetized with isoflurane and perfused with phosphate-buffered saline (PBS), followed by decapitation and rapid brain removal. The cortex and hippocampus of a half hemisphere were dissected out, collected, and quickly frozen for immunoblot analyses. The other hemisphere was fixed with 4% paraformaldehyde for 2 hours at 4°C, then cryoprotected by a transfer to 15% sucrose, followed by 30% sucrose solution in PBS until it sank in the latter. Each hemisphere was briefly dabbed with a lint-free wiper to remove excess sucrose and then rapidly frozen in cooled 2-methylbutane for 30 s on dry ice. Samples were kept at -80°C prior to sectioning and immunohistochemical analysis. All samples were stored at -80^{o}C until further use.

Stereotaxic surgeries

For BAG3 overexpression, 2-month-old P301S male mice received intrahippocampal injections of either AAV9-SYN1-eGFP or AAV9-SYN1-eGFP-2A-hBAG3 in both hemispheres and sacrificed 4 months post injection. Animals received intrahippocampal AAV injections while under isoflurane anesthesia (1.75 % isoflurane in 30/70 % oxygen/nitrogen gas) using a Kopf stereotactic apparatus [16]. Mice were secured using ear bars and a head holder. Ophthalmic ointment was applied to prevent drying of the eyes. Betadine was used to disinfect the scalp prior to incision with a scalpel. A 0.5-mm burr hole was drilled 1.8 mm caudal and 1.8 mm lateral from the bregma.

A 33-GA needle was lowered 2 mm over 2 minutes. A Micro-1 microsyringe pump controller (World Precision Instruments) was used to inject 5 µL of AAVs using the convection-enhanced delivery (CED) method resulting in delivery of approximately 3×10^{11} infection particles/mL into each hippocampus as previously described [42]. The needle was left in place for two additional minutes before it was slowly removed. The burr hole was filled with bone wax (Ethicon, Somerville, NJ), and the incision closed with 50 Dermalon sutures (Covidien, Mansfield, MA). Betadine and topical lidocaine were applied to the top of the suture to prevent infection and for analgesia, respectively.

Cell culture

Primary cortical neurons were prepared from rat embryos at E18 and cultured as previously described with some modifications [35]. In brief, cerebral cortices were isolated from the embryonic rat brains, meninges were removed, then the cortices were transferred into trypsin-EDTA (0.05%) (Corning, MT25053CI). Digestion in trypsin occurred for 15-20 minutes in a 37°C water bath. Following gently trituration, neurons were plated at a density of 100,000 cells/cm^2 for biochemical studies, and at a density of 10,000 cells/cm^2 on coverslips for imaging. Both culture dishes and coverslips were coated with poly-D-lysine (Sigma, P6407). Neurons were grown up to DIV 22 in Neurobasal medium (Thermo Fisher Scientific) supplemented with 2% B27 (Thermo Fisher Scientific) and 2 mM GlutaMax (Thermo Fisher Scientific). Half of the media was replaced every 3-4 days. For lentiviral transduction, DIV7 neurons were treated with virus for 16-24 hours followed by a half medium change.

HEK293T cells (System Biosciences, #LV900A-1) were grown in DMEM medium supplemented with 10% fetal bovine serum (FBS), 2 mM GlutaMax and penicillin/ streptomycin on 60 mm dishes until 80% confluent. HEK cells were transfected with 2-3 µg of the designated construct or empty vector using the PolyJet (SignaGen Laboratories, SL100688).

HEK293T cells were treated with 10 µM YM01 [2] (Sigma #SML0943) or DMSO as vehicle control at for 24 hours before collection for western blot analysis.

Creation of BAG3 null cell line by Crispr/Cas9 system

HEK293T cells were transfected with BAG3 gRNA plasmid (gRNA_eSpCas9-2A- GFP (PX458), GenScript). 20bp gRNA sequence was TCTGTCATGCCGCCACGTAA. Successful delivery of gRNA plasmid was confirmed by visualizing GFP expression. Cells were collected and resuspended in 1ml PBS with 2% FBS. Using fluorescence activated cell sorting (FACS), cells expressing GFP fluorescence were sorted into 96-well plate individually and allowed to grow for

14 days. Cell colonies were expanded, and the knockout of BAG3 was determined by immunoblotting. Tau (0N4R) expressing BAG3 null HEK293TN cells were generated by transducing BAG3 null HEK293TN cells with T4 tau-T2A-RFP expressing lentivirus, followed by fluorescence activated cell sorting.

Lentivirus

To generate lentiviral particles, lentiviral vectors were co-transfected with viral packaging vectors into 70% confluent HEK293TN cells using PolyJet. Media were changed into DMEM containing 1% FetalClone-II serum (Hyclone, SH30066.03) 16h after transfection. The transfected HEK cells were then incubated at 33°C and 5% CO_2 to slow their proliferation. Virus was collected at 64h after transfection and filtered through a 0.2 μm syringe filter to remove cell debris. Viral media was concentrated by ultracentrifugation at 4°C and resuspended in Neurobasal media. Concentrated virus was aliquoted, snap frozen, and stored at -80°C.

Mass Spectrometry Analysis

Rat primary cortical neurons transduced with either pHUUG-Scr or pHUUG-shBAG3 lentivirus at DIV16 were collected at DIV 22. BAG3 antibody (Proteintech, 10599-1-AP) was coupled to Dynabeads using the Dynabeads Antibody Coupling Kit (Thermo Fisher Scientific, Cat # 14311D). Cell lysates were immunoprecipitated with BAG3 antibody coupled beads. After washing, protein was eluted with a low pH elution buffer (0.1M citrate, pH 2.95). 1 M Tris (pH 8.8) was added immediately to the eluate to correct the pH and the samples were submitted to URMC Mass Spectrometry Resource Facility for mass spectrometry analysis.

Samples were run into a 4-12% SDS-PAGE gel to remove contaminants and create a ~10mm length region. These regions were excised, cut into 1mm cubes, de-stained, then reduced and alkylated. Gel pieces were dehydrated and trypsinized at 37°C overnight. Peptides were extracted the next day, then dried down in a CentriVap concentrator (Labconco). Peptides were desalted, dried again, and reconstituted in 0.1% TFA. Peptides were injected onto a homemade 30 cm C18 column with 1.8 um beads (Sepax), with an Easy nLC-1000 HPLC (Thermo Fisher), connected to a Q Exactive Plus mass spectrometer (Thermo Fisher). The Q Exactive Plus was operated in data-dependent mode, with a full MS1 scan followed by 10 data-dependent MS2 scans.

Raw data was searched using the SEQUEST search engine within the Proteome Discoverer software platform, version 2.2 (Thermo Fisher Scientific), using the SwissProt Rattus norvegicus database. Label-free quantitation using Minora was used to determine relative protein abundance

between samples. Percolator was used as the FDR calculator, filtering out peptides which had a q-value greater than 0.01. Identified proteins that showed a greater abundance in the Scr group compared to the shBAG3 group (PSM (Scr/shBAG3)>3) were selected and KEGG analysis was performed with String online platform (string-db.org).

Immunoblotting

Cell or tissue lysates were denatured in 1x SDS sample buffer at 100°C for 10 min before being loaded onto each lane of 10%-15% SDS-PAGE gels. After electrophoresis, proteins were transferred onto nitrocellulose membranes. Membranes were then blocked in TBS-T (0.1% Tween-20) containing 5% non-fat dry milk for 1h at room temperature. Primary antibodies were diluted in blocking solutions followed by incubation at 4°C overnight. The next day, membranes were further incubated with secondary antibody for 1h at room temperature. After thoroughly washing, membranes were visualized by enhanced chemiluminescence and images captured using the KwikQuant™ Imager (Kindle Biosciences, LLC). The intensity of each band was quantified using Image Studio Lite (Li-Cor). GAPDH was used as loading controls. Treatments were then normalized to their corresponding control sample and expressed as a fold difference above the control.

Immunohistochemical staining

Brain slices (30 µm) were prepared from mouse brains fixed with 4% paraformaldehyde using a sliding microtome (VWR 89428-70) with a freezing stage (PhysiTemp Instruments BFS-3MP/PTU-3). The brain sections were washed three times using 0.15 M phosphate buffer (0.05M NaH_2PO_4, 0.1M Na_2HPO_4) to remove the cryoprotectant. Sections were mounted on poly-D-lysine coated slides (Thermo Fisher), antigen retrieval was performed, and the slides were blocked with PBS containing 5% BSA and 0.1% tween 20 for 1 h at room temperature. The sections were incubated with primary antibody in 5% BSA in PBS overnight at 4°C. The next day, slices were incubated for 1 h at room temperature with Alexa Fluor™-conjugated secondary antibody including Alexa Fluor™ 594 donkey-anti-rabbit, Alexa Fluor™ 488 donkey-anti-rabbit, or Alexa Fluor™ 647 donkey-anti-rabbit (Thermo Fisher Scientific). Alternatively, they were labeled using the MOM kit (BMK-2202, Vector laboratories), followed by three washes with PBS and labeling with Streptavidin Alexa Fluor™ 488 or 647 (Thermo Fisher Scientific). The brain sections were coverslipped with ProLong Diamond Antifade Mountant (Thermo Fisher Scientific, P36961). The slides were imaged using a Nikon A1R HD laser scanning confocal microscope (Nikon). The brain sections were imaged at CA1 of hippocampus with Nikon ECLIPSE Ti2 and recorded by NIS-Elements (Version 5.11) software. Resulting images were pseudocolored for illustration purposes.

Immunofluorescence

Neurons grown on coverslips were rinsed with PBS twice and followed by fixing in PBS containing 4% paraformaldehyde and 4% sucrose for 5 minutes at room temperature. Then, neurons were permeabilized in PBS containing 0.25% Triton X-100 and were blocked with PBS containing 5% BSA and 0.3 M glycine. Primary antibodies were diluted in blocking solution, added to the coverslips, and incubated on a shaker at 4°C overnight. Alexa Fluor 488/594/647 conjugated secondary antibodies were diluted in blocking solution and incubated with neurons for 1 hour at room temperature. Coverslips were counterstained with Hoechst 33342 and mounted with ProLong Diamond Antifade Mountant. Images were acquired on a Nikon A1R HD scanning confocal microscope using a 40x objective with a 2x optical magnification. Resulting images were pseudocolored for illustration purposes.

Live cell imaging

BAG3 null HEK293TN cells on 25mm coverslips were transfected with control vector or BAG3 expression vector together with GFP-Rab35 and Hrs-RFP. The coverslips were placed in an Attofluor™ Cell Chamber (#A7816, Thermo Fisher Scientific) with Krebs-Ringer Solution at 36 hours post transfection. During imaging, cells were placed inside a heating chamber (TIPA plate adapter for Nikon TIA) at 37 °C. Live cell imaging of fluorescent proteins was performed using a Nikon A1R HD laser scanning confocal microscope and images were acquired with a 60x Oil objective. Images obtained by Nikon ECLIPSE Ti2 and recorded by NIS-Elments (Nikon, Version 5.11) software at a rate of 6 frame per minute for 10 minutes.

Live cell image stacks were analyzed using Imaris Cell Imaging Software (Bitplane, Switzerland). Briefly, kymographs were generated using the function of swap time and z, and the rendered images were rotate 45 degree. The mobility of Hrs-RFP was determined by using the spots module in Imaris. First spots were generated for the Hrs-RFP range of 1~2μm in diameter. Next, the spots were tracked over 10 minutes and the track of the spots were recorded. Finally, the total length of the different tracks was binned every 0.1 μm. Over 10 cells for each group were used for analysis.

Immunoprecipitation

Cells were lysed in ice-cold lysis buffer (50 mM Tris, 150 mM NaCl, 0.4% NP-40, 1 mM EDTA, 1 mM EGTA, pH7.4) supplemented with protease inhibitor cocktails and phosphatase inhibitors. Cell lysates were briefly sonicated then centrifuged at 13,200 rpm for 10 minutes at 4°C. Cleared supernatants (500 μg) were mixed with 2 μg normal rabbit/mouse IgG control or primary antibody,

followed by incubation at 4°C for 24h. Antibody/antigen mixture was incubated with Dynabeads M-280 sheep anti-rabbit or mouse IgG (Thermo Fisher Scientific) for 6h at 4°C on the following day. An aliquot of protein lysate was saved for input control. After thoroughly washing the beads, bound fractions were eluted in sample loading buffer by boiling at 100°C for 10 minutes. Proteins were then resolved by SDS-PAGE. To reduce the background of heavy chain and light chain from IgG and antibodies, a conformation specific mouse anti-rabbit IgG, a secondary rabbit antibody, was used following the precipitation of TBC1D10B.

Rab35 activity assay

The Rab35 activity assay was performed as previously described [46]. Briefly, pGEX (GST only) or pGEX-RBD35 were transformed into BL21 E. coli, and GST and GST-RBD35 protein expression was induced with IPTG, followed by purification using glutathione S-transferase beads (Ge healthcare, #17-5132). The proteins were eluted and concentrated with Amicon Centrifugal Filter Units 10K (GST) and 50K (GST-RBD35) (Millipore) to remove excessive glutathione. Cell lysates from 10 cm dishes were collected and incubated with 1.25 μg of GST or GST-RBD35 recombinant protein, followed by precipitation with glutathione S-transferase beads. The precipitated samples were analyzed by immunoblotting and 1~4% of the cell lysates were used as input controls.

Image analysis

Immunofluorescence images were opened and processed with combination of Image J and Imaris. Region of interests were either selected around the soma, or a line (line width equals 120 pixels) was drawn along processes, followed by straightening with Imaris. Line scans were generated using the plot profile tool in Fiji (line width of one pixel). Intensity values for a given marker were normalized by subtracting the minimum background and dividing the dataset by its maximum.

Colocalization analysis was done using Imaris. Specifically, regions of interest were selected at the molecular layer in the CA1 region of the hippocampus (Fig 2b, Fig 9 a and b) or along processes with a line width of 200 pixels, followed by straightening (Fig 2c-f, Figs 6a, Fig 7a and d). Co-localization module was used, and different fluorescence channels were thresholded to generate a new colocalization channel. Mander's colocalization coefficients were used to quantify the overlapping of fluorescence intensity[1].

Western blot images were turn into Black and white with photoshop software (Adobe, Ver, CC). And the grey value was analyzed with image studio lite (LI-COR Biosciences, Ver 5.0).

Statistical analysis

All image measurements were obtained from the raw data. GraphPad Prism was used to plot graphs and perform statistical analysis. The statistical tests used are denoted in each Figure legend, and statistical significance was defined as *$p < 0.05$ and **$p < 0.01$. For the live-cell imaging analysis, the difference of Hrs mobility curves (Fig 6d) was transformed into an accumulation curve and then analyzed using the Kolmogorov–Smirnov test.

Results

BAG3 plays an essential role in the clearance of tau and other disease-relevant aggregation-prone proteins [27,8,51,9]. Our previous findings, together with those from other groups, have focused on BAG3's role in autophagy [51,36]. However, as a co-chaperone protein with multiple domains, BAG3 likely has regulatory functions beyond autophagy through its interaction with other proteins. To better understand the role of BAG3 in mediating these processes, we immunoprecipitated endogenous BAG3 from mature neuron cultures transduced with either scrambled or shBAG3 shRNA. By comparing the mass spectrometric analysis data from the scrambled and shBAG3 transduced neurons, we identified 127 proteins (peptide-spectrum match (PSM): (Scr/shBAG3)>3) that were enriched in the BAG3 precipitates from scrambled transduced neurons compared to shBAG3 transduced neurons, thus indicating an association with BAG3 (Supplementary Table). We further validated several of the BAG3 interactors, including MAP6 and clathrin heavy chain, by immunoprecipitating BAG3 from rat neurons transduced with lentivirus expressing scrambled or shBAG3 shRNA followed by immunoblotting (Fig s1, a and b). To identify the functional categories of the BAG3's interactors, we used KEGG analysis and found the top pathway is the endocytosis pathway (Fig 1a). With string analysis, we found a cluster of endocytosis-related genes that interact with each other and are closely related to a group chaperone and co-chaperone protein (Fig 1b and Fig s2). Among the genes associated with endocytosis, there are three main groups, including chaperone proteins, cytoskeletal proteins, and proteins that modulate the activity of small GTPases. In this last category, we were very excited to find TBC1D10B (also known as EPI64B or FP2461), which is a GAP for Rab35 [31]. Rab35 is an essential Rab that controls endocytosis, recycling of synaptic vesicles, neurites elongation [45,66], and the targeting of tau to the endolysosome compartment [72]. Given the pivotal role of Rab35 in mediating vacuolar processes, neuronal health and tau clearance, we focused on defining the interaction of BAG3 with TBC1D10B and the functional implications of this interaction.

BAG3 interacts with TBC1D10B in hippocampal and cortical neurons.

To verify the predicted interaction of TBC1D10B with BAG3, we immunoprecipitated TBC1D10B from rat cortical neuron lysates and immunoblotted for BAG3. Endogenous BAG3 readily co-precipitated with TBC1D10B (Fig 2a). We next investigated the spatial localization of BAG3 and TBC1D10B in mouse brain. Immunohistochemistry (IHC) of 8-month-old wildtype mouse brain sections show TBC1D10B co-localizes with BAG3 predominantly in punctae in soma and neurites in the CA1 region of the hippocampus (Fig 2b). We further examined the colocalization of BAG3 with TBC1D10B in cultured rat cortical neurons. Similar to what was observed in vivo, TBC1D10B co-localized with BAG3 in the neurites and the soma in punctate-like structures (Fig 2 c-g). Colocalization analysis [1] showed that 12.4 ± 2.8% (Mean ± SEM) of TBC1D10B-positive puncta co-localized with BAG3 in the soma and 8.0 ± 2.0 % (Mean ± SEM) in the neurites of the primary cultured neurons (10 neurons from each group were used for analysis). These data suggest BAG3 and TBC1D10B are associated with each other in both hippocampal and cortical neurons.

The interaction of BAG3 with TBC1D10B is facilitated by HSP70.

BAG3 is a co-chaperone protein with multiple domains [69] and therefore, we wanted to define the domains that are necessary for its interaction with TBC1D10B. FLAG-tagged TBC1D10B was co-expressed with wild-type (WT) BAG3, WAWA BAG3 (mutation at the WW domain of BAG3 in the N terminal which is required for interaction with synaptopodin) [36], GPG BAG3 (mutation at both IPV domains of BAG3 where small heat shock proteins bind)[26,9], or L462P BAG3 (mutation in the C terminal BAG domain which is where Hsp70 binds) [20,3] in BAG3 null cells, followed by immunoprecipitation with a FLAG antibody. The data show that the WAWA mutation of BAG3 slightly decreased its association with TBC1D10B (Fig 3a). However, the L462P mutation of BAG3 almost abolished its interaction with TBC1D10B (Fig 3a). L462P is a rare mutation that causes dilated cardiomyopathy [3] and prior in vitro studies have suggested that L462P BAG3 does not efficiently bind HSP70 (data not shown). Since the L462 site is likely necessary for BAG3 to effectively bind with HSP70, we hypothesized that HSP70 may be involved in the association of BAG3 with TBC1D10B. We first verified that the L462P mutation of BAG3 decreases its association with HSP70. WT BAG3 or L462P BAG3 was co-transfected with V5-HSP70 into BAG3 null HEK cells, followed by immunoprecipitation with V5 and immunoblotting for BAG3. Our data demonstrate that the association of HSP70 with L462P BAG3 was reduced over 53% compared with WT BAG3 (Fig 3b), confirming the dependence of the L462 site of BAG3 for the association. To examine how HSP70 regulates the association of BAG3 with TBC1D10B, FLAG-TBC1D10B was co-transfected with V5-HSP70 or empty vector into HEKs cells followed

by immunoprecipitation with the FLAG antibody. We found overexpression of HSP70 enhanced the association between BAG3 and TBC1D10B (Fig 3c). We further asked if disruption of the association between BAG3 and HSP70 could affect the association of TBC1D10B with BAG3. We co-transfected FLAG-TBC1D10B together with V5-HSP70 or empty vector into HEK cells, followed by treatment with YM01, which locks HSP70 in the ADP bound state and reduces its binding to BAG3 [53]. Cell lysates were immunoprecipitated with the FLAG antibody and blotted for BAG3. We found that YM01 treatment disrupted the association of BAG3 with TBC1D10B. Interestingly, expression of exogenous HSP70 leads to less disruption of BAG3-TBC1D10B interactions by YM01, which may due to saturation of YM01 by excessive HSP70 (Fig 3d). Overall, these findings suggest HSP70 facilitates the association of BAG3 with TBC1D10B. These findings further prompted us to examine if HSP70 could associate with TBC1D10B independent of BAG3. We co-transfected FLAG-TBC1D10B and V5-HSP70 in BAG3 null HEKs cells, followed by immunoprecipitation with V5 antibody. Our data showed HSP70 associates with TBC1D10B in the absence of BAG3 (Fig 3e). BAG3 interaction with HspB8 prevents its degradation resulting in increased stability [9,25] and the same is most likely true for HSP70, as increased expression of BAG3 greatly increases HSP70 levels (Fig 3f). To examine if BAG3 could also regulate the association between HSP70 with TBC1D10B, we co-transfected V5-HSP70, FLAG-TBC1D10B, and WT BAG3 or empty vector followed with a saturated immunoprecipitation with the V5 antibody. This resulted in equal amounts of V5-HSP70 in the control and BAG3 overexpression group when pulled down with V5 (Fig 3g). These data demonstrated that BAG3 greatly enhances the association of HSP70 with TBC1D10B. Overall, our data indicate that HSP70 facilitates the association of BAG3 and TBC1D10B, and that HSP70, TBC1D10B and BAG3 interact to form a complex.

BAG3 regulates the Rab35 activity through the association of TBC1D10B.

TBC1D10B is a GAP that specifically associates with the GTP bound, active form of Rab35 and promotes GTP hydrolysis, leading to the inactivation of Rab35 [31]. Since our data showed that BAG3 associates with TBC1D10B, we examined how BAG3 may regulate the function of TBC1D10B. Rat cortical neurons were transduced with lentivirus expressing scrambled or shBAG3 shRNA, followed by immunoprecipitation of TBC1D10B and immunoblotting for Rab35. Our data showed that depletion of BAG3 doesn't change the protein level of TBC1D10B, but instead inhibits the association of TBC1D10B with Rab35 (Fig 4a). This finding leads to two opposing hypotheses: hypothesis 1; Because GAPs preferentially bind GTP bound Rabs[63,81]. BAG3 promotes the association of TBC1D10B with Rab35, which leads to the inactivation of

Rab35 (conversion to GDP-Rab35) and thus decreases in Rab35 that immunoprecipitates with TBC1D10B; hypothesis 2, Binding of BAG3 attenuates the ability of TBC1D10B to stimulate the GTPase activity of Rab35, and resulting in prolonged association of TBC1D10B with Rab35 [59]. To test these hypotheses, we used an established Rab35 activity assay. We generated GST tagged RBD35, which specifically binds the active, GTP-bound form of Rab35 [46]. Cell lysates from rat neurons transduced with lentivirus expressing scrambled or shBAG3 shRNA were incubated with GST or GST-RBD35 on glutathione beads, with the precipitates blotted for Rab35. Our data show that knockdown of BAG3 doesn't change the expression level of Rab35; instead, it reduces the activity of Rab35 (Fig 4b). This finding supports our second hypothesis that BAG3 keeps Rab35 in a GTP-bound state by associating with TBC1D10B, which prevents the inactivation of Rab35. To examine if disrupting the association of BAG3 with TBC1D10B could also affect Rab35 activity, we co-transfected Myc-Rab35 with WT BAG3, L462P BAG3, or empty vector in BAG3 null HEKs. Rab35 activity assay results showed that loss of BAG3 substantially decreases the level of GTP bounded Rab35 without affecting its expression level, which is consistent with our finding in rat cortical neurons (Fig 4c). Interestingly, the L462P mutation of BAG3, which greatly disrupts its association with TBC1D10B, also decreased the level of GTP-bounded Rab35 (Fig 4c). Our findings suggest that BAG3 associates with TBC1D10B in order to maintain Rab35 in an active state. In contrast, depletion of BAG3 or freeing TBC1D10B from BAG3 will increase the inactivation of Rab35. This finding further leads to another hypothesis that a primary mechanism by which BAG3 regulates the Rab35 activity is through mediating the function of TBC1D10B. To test this hypothesis, we examined Rab35 activity under the conditions of the knockdown of BAG3 or TBC1D10B, or both BAG3 and TBC1D10B. Our data demonstrate that Rab35 activity is decreased when BAG3 is knocked down and increased when TBC1D10B is knocked down compared with scrambled controls. The decreased activity observed with BAG3 knockdown was alleviated when TBC1D10B was knocked down as well (Fig 4d). These findings show that the BAG3 regulates Rab35 activity through its interaction with its GAP, TBC1D10B.

BAG3 interacts with TBC1D10B to regulate tau sorting into the endocytic pathway through the ESCRT system.

Rab35 is a GTPase that plays an essential role in the endocytic pathway and facilitates tau clearance in neurons [72]. As shown in primary rat cortical neurons, BAG3 promotes tau degradation [51] and interacts with TBC1D10B (Fig 2a). This association with TBC1D10B ultimately regulates the activity of Rab35 (Fig 4b), which leads to TBC1D10B potentially playing a role in phosphorylated tau clearance as well. Indeed, our data shows that depletion of

TBC1D10B in neurons significantly decreased the level of p-Thr231, p-Ser262, and p-Ser396/Ser404 tau in mature neurons (Fig 5a and b). We also examined if depletion of TBC1D10B would rescue the accumulation of tau caused by knockdown of BAG3 (Fig 5c). Our data show that knockdown of BAG3 increases the level of p-Thr231, p-Ser262, and p-Ser396/Ser404 tau in mature neurons, confirming our previous results [51]. However, depletion of both TBC1D10B and BAG3 significantly reduced the increases in phosphorylated tau compared with knockdown of BAG3 alone (Fig 5d and e). These data suggest that TBC1D10B is downstream of BAG3 in regulating tau clearance. As indicated by our mass spectrometry analysis, BAG3 is involved in regulating the endocytic pathway (Fig 1a). Further, Rab35 has been shown to facilitate phosphorylated tau clearance through the ESCRT system [72]. Therefore, we hypothesized that BAG3 collaborates with TBC1D10B to regulate phosphorylated tau clearance through the ESCRT system. In initial studies, we examined the colocalization between CHMP2B, an ESCRT-III component [67], and p-Ser396/404 tau in neuronal processes. In the shBAG3 group, p-Ser396/404 tau colocalization with CHMP2B was significantly decreased compared with the scrambled group. Depletion of both BAG3 and TBC1D10B significantly increased the colocalization of p-Ser396/404 tau with CHMP2B (Fig 6). These findings indicate that BAG3 interacts with TBC1D10B to regulate phosphorylated tau clearance through the ESCRT system.

BAG3 regulates the recruitment of Hrs to Rab35.

Rab35 plays an essential role in the ESCRT system. When activated, Rab35 recruits Hrs, an ESCRT 0 component, to the surface of the endosome. This not only facilitates the recruitment of the ESCRT machinery to form intraluminal vesicles, but also plays a role in directing cargo to the endosome for engulfment [66], and a previous study provided evidence that these cargos include various phospho-tau species [72]. Since our data suggest that BAG3 regulates the activity of Rab35 through interacting with TBC1D10B, we hypothesize that BAG3, by promoting active Rab35, should facilitate the recruitment of Hrs to Rab35. Therefore, we investigated the colocalization of Rab35 with Hrs in primary rat cortical neurons. We found Rab35 co-localizes with Hrs both in the soma and neuronal process in the scrambled group, whereas colocalization was significantly decreased in BAG3 knockdown neurons (Fig 7 a-f). The recruitment of Hrs to Rab35 to initiate the ESCRT pathway is a dynamic process, in that Hrs must be both recruited and released for intraluminal vesicle formation of MVBs [73]. To examine the dynamics of Rab35 and Hrs, we co-transfected eGFP-Rab35 and Hrs-RFP together with WT BAG3 or empty vector in BAG3 null HEKs. When BAG3 was absent, we observed that majority of Hrs puncta were stationary, and 4.5% of the Hrs puncta moved more than 1μm during the 10-minute imaging

session (Fig 7g and h). With the presence of BAG3, Hrs puncta were mobile and 23% of the Hrs puncta moved more than 1μm during the 10-minute imaging session (Fig 7g and h). Additionally, we observed the colocalization of Rab35 with Hrs was greatly increased in the presence of BAG3 compared with the BAG3 null condition (Fig 7 i). These findings suggest BAG3 enhances the mobility of Hrs and boosts the recruitment dynamics of Hrs to Rab35. Next, we examined the regulatory function of BAG3 and TBC1D10B on the association of Hrs and Rab35 by expressing Myc-Rab35 with/without BAG3 and TBC1D10B in BAG3 null HEKs cells, followed by immunoprecipitation with a Myc antibody. Our immunoprecipitation result showed Rab35 and Hrs barely associate with each other in the BAG3 null condition, while this association was greatly enhanced with the presence of BAG3 (Fig 7j). Further, overexpression of TBC1D10B disrupts the association of Rab35 with Hrs in the presence of BAG3 (Fig 7j). These findings suggest BAG3 strongly promotes the recruitment of Hrs to Rab35, and TBC1D10B acts downstream of BAG3 to inhibit this recruitment. As specific domains of BAG3 were involved in mediating its interaction with TBC1D10B, we hypothesized that mutations of BAG3 in the different domains may affect the recruitment of Hrs to Rab35. Since Hrs recruitment is important to initiate the ESCRT pathway to sort tau into endosome-lysosome for degradation [4,73,72], we also hypothesize that mutations of BAG3 may affect tau degradation in a domain-dependent manner. To test these hypotheses, we generated stable tau-expressing BAG3 null HEKs cells by transfecting BAG3 null HEKs cells with 0N4R tau-T2A-RFP, followed by fluorescence-activated cell sorting. We then transfected Hrs, Myc-Rab35, and WT BAG3 or BAG3 with different mutations into the BAG3 null HEKs cells. Our data showed expression of WT BAG3, WAWA BAG3, or GPG BAG3 significantly reduced tau levels in BAG3 null HEKs (Fig 7k and l). However, expression of L462P BAG3 did not result in a significant decrease in tau levels, demonstrating the importance of the BAG domain of BAG3 in tau degradation (Fig 7g and h). Next, we immunoprecipitated Myc-Rab35 and blotted for Hrs. We found that expressing WT BAG3, WAWA BAG3 or GPG BAG3 enhanced the association of Hrs with Rab35 compared with the BAG3 null condition, while the L462P BAG3 expression group barely showed any association of Hrs with Rab35 (Fig 7m). Since the L462P mutation of BAG3 disrupts the association of BAG3 and TBC1D10B, our findings indicate that BAG3 collaborates with TBC1D10B to regulate the Hrs recruitment to Rab35.

Hippocampal overexpression of BAG3 alleviates the tau pathology development in P301S mice.

BAG3 is essential for maintaining proteostasis and increases in neurons during the aging process [71], and a recent report indicated that BAG3 levels are likely decreased in AD brains compared

to aged matched controls [82]. Further, previous studies suggest that overexpression of BAG3 in rat cortical neuron promotes tau clearance [51]. Given these findings, we hypothesize that increases in BAG3 levels may alleviate tau pathology development. To determine the effect of increasing BAG3 overexpression on tau pathology, we used P301S mice (PS19 line) [79]. For these studies we only used male P301S as it has been reported that they develop tau pathology more consistently than females [56,80]. Two-month-old P301S mice were administered bilateral intrahippocampal AAV injections of hBAG3 (with an N-terminal FLAG-Myc tag) or empty vector control (both AAVs also express eGFP) and collected at 6 months of age. IHC data showed endogenous BAG3 is expressed both in the soma and neurites of the CA1 region of the control brain (Fig 8a), with levels of BAG3 significantly increased in the BAG3 overexpression group. Exogenous BAG3 is mainly expressed in the hippocampal region as shown by Myc-tag staining (Fig 8a). Western blot analysis of hippocampal lysates show that the BAG3 levels in the BAG3 overexpression group are significantly elevated and approximately four-fold of that of the control group (Fig 8b and c). However, the BAG3 level is not changed in the cerebellum region, indicating the regional specificity of BAG3 overexpression (Fig s3 a and b). Next, we investigated the function of BAG3 in modulating the tau levels of P301S mice. Immunoblots of hippocampal lysates showed total human tau (recognized by the human tau specific antibodies HT7 [19] and 5A6 [39]) were significantly decreased in the BAG3 overexpression group (Fig 8d and e). We further examined the phosphorylated tau species in these lysates. Immunoblot data of the hippocampal lysates showed that the levels of p-Ser262 tau, p-Thr231 tau and p-Ser396/404 tau were significantly decreased in the BAG3 overexpression groups compared with the AAV control groups (Fig 8f and g). Total human tau levels were not significantly changed between the control and BAG3 overexpression groups in the cerebellum, indicating the decrease in tau is closely related to BAG3 overexpression (Fig s3c and d). Quantitative IHC also showed p-Ser262 tau and p-Ser396/404 tau were significantly decreased in the CA1 region in the BAG3 overexpression brains (Fig 8h and i). Moreover, we also examined oligomeric tau with the T22 tau antibody [50]. The percentage of T22 positive cells was significantly reduced in the BAG3 overexpression group compared with the control group (Fig 8j). Staining with the conformation-dependent MC1 tau antibody [38] was also decreased in CA1 region of the hippocampus when BAG3 was overexpressed (Fig 8k). These findings suggest that overexpression of BAG3 reduced the level of pathogenic tau species in P301S mice hippocampus and indicates an essential role for BAG3 in tau clearance.

We further tested our hypothesis that BAG3 promotes the recruitment of Hrs to Rab35 in vivo. Co-immunostaining of Hrs and Rab35 in the P301S mouse brains showed significantly more

Rab35 co-localized with Hrs in the CA1 region in the BAG3 overexpression group compared with the control group (Fig 9 a-c). Furthermore, co-immunostaining of p-Ser396/404 tau with ESCRT-III component, CHMP2B, showed colocalization of p-Ser396/404 tau with CHMP2B was significantly increased in the BAG3 overexpression group (Fig 9 d-f). Finally, we examined the role of BAG3 in the synapse loss of P301S mice [79]. IHC staining for MAP2 and PSD95 was used to visualize dendrites and postsynaptic compartments, respectively [33,6]. To quantify the density of MAP2 and PSD95, the images were reconstructed using the Imaris Surface Rendering Model. Our data showed the MAP2 and PSD95 density was significantly increased in the BAG3 overexpression group (Fig 10a-c). Overall, these findings suggest hippocampal overexpression of BAG3 alleviates tau pathology development in P301S mice.

Discussion

Proteostasis is an essential aspect of neuron health that becomes less functional during aging, the primary risk factor for AD [43]. Dysregulation of proteostasis in neurons will lead to the accumulation of pathologic proteins, with phosphorylated tau species being a defining characteristic of AD [48]. Given that pathological tau species are essential factors in the development and progression of AD [78,41], facilitating the clearance of these tau species by manipulating autophagy and endolysosomal pathways could be part of a potential therapeutic strategy [34]. Previous studies from our lab demonstrated that BAG3 regulates the clearance of phosphorylated tau through the autophagy pathway [51,36]. To determine if BAG3 may function to regulate protein clearance pathways beyond autophagy, we carried out an unbiased proteomic analysis to identify interactors of endogenous BAG3 in neurons. The results of this screen revealed that BAG3 directs a novel regulatory mechanism of the endolysosomal pathway that facilitates the removal of phosphorylated tau species. Indeed, the primary pathway represented by the proteins that co-precipitated with endogenous BAG3 was the endocytic pathway, with one of these proteins being the Rab35 GAP, TBC1D10B. The interaction of BAG3 with TBC1D10B increases Rab35 activity and its dynamic association with Hrs. This is a fundamentally important process that results in ESCRT-mediated targeting of tau to the endosome for eventual clearance by the lysosome [72]. Further, our data suggest the association of BAG3 with HSP70 is essential for its regulatory function of TBC1D10B. This finding is novel as it is the first to implicate the BAG3-HSP70 complex in regulating the Rab GTPase cycle. Moreover, our in vivo study using intrahippocampal delivery of BAG3 in P301S tau mice resulted in significantly decreased tau levels concomitant with an attenuation of synaptic loss and decreased neuronal atrophy.

BAG3 is a co-chaperone protein that plays an essential role in proteostasis. BAG3 is increased with aging [71]. However, recent data suggest that BAG3 expression is decreased in human AD brains compared with the aged control [82]. A previous study in our lab showed that depletion of BAG3 in rat cortical neurons increased the levels of endogenous phosphorylated tau [51]. The present study is the first to examine the function of BAG3 in tau clearance in a tauopathy mouse model. Recent data suggest that the 0N and 4R isoforms of tau are most likely to aggregate in AD [74] and intriguingly 0N4R tau with the P301S mutation is what is overexpressed (~5x over endogenous) in the PS19 mice which were used in this study [79]. In the present study, we observed BAG3 expression in the hippocampus reduces both human total tau and phosphorylated tau species, suggesting the essential role of BAG3 in tau clearance. We noticed that the overexpression of BAG3 also increased the density of dendrites and postsynaptic compartments in the P301S mice. This finding echoes the results from a recent study indicating that exogenous expression of BAG3 in the 5XFAD mouse model increased the expression of synaptic proteins [82].

BAG3 is a protein with multiple domains and numerous binding partners, which results in modulating the function of various cellular processes [44]. For example, the C-terminal BAG domain interacts with the ATPase domain of HSP70 [68], the N terminal WW domain mediates binding with synaptopodin [36], and the IPV domains mediate binding to HspB6 and HspB8[26]. An earlier global analysis of BAG3 interacting partners in Hela cells using quantitative immunoprecipitation showed enrichment in proteins functioning within the ubiquitylation-proteosome pathway [15]. In contrast, our findings in primary rat cortical neurons showed endogenous BAG3 co-precipitated with proteins from the endocytic pathway, rather than the ubiquitylation-proteasome system. These results suggest BAG3 may play different roles in different cell types [70,21,36]. Another recent study using rat neurons in which GFP-BAG3 (or GFP only) was overexpressed for 72 hours, followed by immunoprecipitation with a GFP antibody. The mass spectrometric analysis showed BAG3 interactors enriched in the synaptic vesicle cycle [82]. The fact that in this previous study, a different set of BAG3 interactors was identified compared to our present study (although there were a few proteins in common) could be due the overexpression of BAG3 altering protein-protein interactions. It can be speculated that overexpression of BAG3 will likely greatly enhance the expression of HSP70 and stabilize it in an active form [64,62], which also may result in a different interactors co-precipitating. In addition, the fact that they used GFP overexpression as a control, while we used depletion of BAG3 by transducing neurons with shBAG3 as our control, could also be a contributing factor to the differential co-immunoprecipitation protein binding profile. Further studies are needed to elucidate

the specific reasons for these differences. Nonetheless, given that we identified proteins that interacted with endogenous BAG3 in neurons and used neurons with BAG3 knocked down to increase the stringency of our screen strongly supports the validity of our findings. In addition, we found that known interactors of BAG3 such as HspB8 [9], HSC70 (HspA8) [30] and 14-3-3γ [76] co-immunoprecipitated with endogenous BAG3 in our study (Supplementary Table).

TBC1D10B, also known as EPI64B or FP2461, belongs to TBC1 protein family, which mainly function as GAPs promoting GTP hydrolysis and selective inactivation of the different Rab proteins [24]. In the present study, we identified TBC1D10B as a BAG3 interactor and demonstrated the importance of this interaction in regulating endocytic pathways. Further, we found that the L462P mutation at the BAG domain, which is where HSP70 also binds [68], disrupts the association of BAG3 with TBC1D10B. Since HSP70 promotes the association of BAG3 with TBC1D10B, and HSP70 is able to bind TBC1D10B independent of BAG3, our data support a regulatory model of the association of HSP70 with BAG3 promoting its interaction with TBC1D10B. It should also be noted that BAG3 overexpression greatly increased the expression level of HSP70 and promoted the association of HSP70 and TBC1D10B (Fig 3 f, g). This could be explained by BAG3's role in stabilizing HSP70 in an activated form [64,62], which may favor the association of HSP70 with TBC1D10B.

Rab35 is a key player involved in multiple cellular functions, including endosomal trafficking[47], ESCRT mediated tau degradation[72], presynaptic protein homeostasis [66], and neurite outgrowth[17]. As a GTPase, Rab35 acts as a molecular switch that cycles between active (GTP-bound) and inactive (GDP-bound) states. Active Rab35 recruits effectors that regulate the endocytic pathway to recycle different cargos [45]. A recent study also found Rab35 regulates the degradation of synaptic vesicle proteins in a activity-dependent manner [66]. In the present study, we found BAG3 enhances the association of TBC1D10B with Rab35, while knocking down of BAG3 decreased Rab35 activity. TBC1D10B, as a GAP, preferably binds with the active form of Rab35 and subsequently promotes the inactivation of Rab35 [46]. These findings suggest a regulatory model in which the binding of BAG3 to TBC1D10B attenuates the ability of TBC1D10B to stimulate the GTPase activity of Rab35, resulting in activation of Rab35 [59]. Interestingly, we also noticed that the L462P mutation of BAG3, which disrupts the association of HSP70 with BAG3, decreased Rab35 activity. Given that BAG3 is a nucleotide exchange factor (NEF) and thus activates HSP70 [64,62], which also interacts with TBC1D10B, suggests that BAG3 activates HSP70 and enhances its binding with TBC1D10B. During this process, the ability of TBC1D10B to promote the GTPase activity of Rab35 was attenuated, which in turn to keeps

Rab35 in an activated form [46]. As a result, BAG3 promotes the association of TBC1D10B with Rab35, but also keeps Rab35 in an activated state at the same time.

ESCRT complexes orchestrate the endolysosome pathway and thus are essential components of the neuronal proteostasis network [28]. Activated Rab35 recruits Hrs, an ESCRT 0 component, to the endosome and thus initiates the ESCRT pathway, MVB formation, and clearance of the targeted cargo [72,66]. Hrs binds to both ubiquitylated and non-ubiquitylated cargos, including tau proteins, and sorts them to the endosome for eventual degradation [22,77,72]. It should also be noted that both Rab35 activation/deactivation and the recruitment of Hrs to the endosome are dynamic processes. The dynamics of Hrs recruitment and release defines the timing and morphology of intraluminal vesicle formation [73]. In our present study, we found BAG3 regulates the association and colocalization of Rab35 with Hrs, and this may be due to the regulatory role of BAG3 on the activity of Rab35. BAG3 also regulates Hrs mobility and dynamic colocalization with Rab35, as shown by live-cell imaging. Since every time Hrs dwells on an endosome intraluminal vesicle formation can be initiated, the high mobility and frequency of interaction of Rab35 with Hrs will promote ESCRT-mediated sorting of cargo into endosome and maturation of MVBs [72,66]. This is also consistent with our in vivo finding that BAG3 overexpression increases the co-localization of Rab35 with Hrs and Hrs with p-Ser396/404 tau. These data suggest a mechanism that BAG3 regulates the activity of Rab35 to promote the ESCRT mediated tau clearance. Interestingly, we also noticed L462P mutation of BAG3 or overexpression of TBC1D10B greatly disrupts the association of Rab35 with Hrs. These findings suggest that BAG3 collaborates with HSP70 and TBC1D10B to regulate the recruitment of Hrs by Rab35.

In conclusion, the results of our study describe for the first time a BAG3-HSP70-TBC1D10B signaling axis that modulates Rab35 activity and thus ESCRT-mediated endosomal tau clearance. During normal aging, increased BAG3 promotes the association of BAG3-HSP70-TBC1D10B, thus the inactivation function of TBC1D10B on Rab35 is prohibited. The activation of Rab35 recruits Hrs, which initiates the ESCRT mediated endosomal tau clearance. In AD brains, however, this increase of BAG3 may be attenuated, which would release TBC1D10B from the BAG3-HSP70-TBC1D10B complex. The TBC1D10B will thus be free to inactivate Rab35, which could contribute to an accumulation of phosphorylated tau (Fig 11). Given the key role that Rab35 plays in regulating vacuolar-dependent processes, it is likely that this BAG3 signaling complex extends beyond tau clearance mechanisms. Overall, the present study on BAG3 illustrates the fundamental importance of understanding the functions of BAG3 in maintaining healthy neurons

during aging and how these processes may be dysregulated in AD and other neurodegenerative diseases.

Acknowledgements: We thank Dr. C.Pröschel, University of Rochester for providing us with the pHUUG vector; Dr. J. Höfeld, University of Bonn for providing us with BAG3, L462P BAG3 and WAWA BAG3 in pcDNA; Dr. L.I. Binder for the gift of the MAP2 and tau5 antibodies (AP14) [31, 32]; Dr. P. Davies for the gift of MC1 and phospho-Tau (Ser396/404) (PHF1) antibodies; Dr. P. Dolan for the gift of phospho-Tau (Ser262) antibody. This work was supported by National Institute of Health (NIH) grants R56 AG067739 and R01 NS098769. This research has been facilitated by a fee for service provided by the University of Rochester Mass Spectrometry Resource Laboratory and NIH instrument grant (S10OD021486).

Author contributions: GJ contributed to the study conception and design, edited the manuscript, and provided funding. HL contributed to the study conception and design, performed experiments, analyzed the data, interpreted the experiments, wrote the manuscript. MT, CJ contributed to the study conception and design, performed experiments, analyzed the data and edited the manuscript. PG, GC, YC performed experiments, analyzed the data and edited the manuscript.

Compliance with ethical standards

Conflict of interest The authors declare that they have no conflicts of interest with the contents of this article.

Ethical approval: All the work involving animals was reviewed and approved by the University Committee on Animal Research of the University of Rochester. (Protocol #:2007-023E&ER).

References

1. Aaron JS, Taylor AB, Chew TL (2018) Image co-localization - co-occurrence versus correlation. Journal of cell science 131. doi:10.1242/jcs.211847
2. Abisambra J, Jinwal UK, Miyata Y, Rogers J, Blair L, Li X, Seguin SP, Wang L, Jin Y, Bacon J, Brady S, Cockman M, Guidi C, Zhang J, Koren J, Young ZT, Atkins CA, Zhang B, Lawson LY, Weeber EJ, Brodsky JL, Gestwicki JE, Dickey CA (2013) Allosteric heat shock protein 70 inhibitors rapidly rescue synaptic plasticity deficits by reducing aberrant tau. Biological psychiatry 74:367-374. doi:10.1016/j.biopsych.2013.02.027
3. Arimura T, Ishikawa T, Nunoda S, Kawai S, Kimura A (2011) Dilated cardiomyopathy-associated BAG3 mutations impair Z-disc assembly and enhance sensitivity to apoptosis in cardiomyocytes. Hum Mutat 32:1481-1491. doi:10.1002/humu.21603
4. Bache KG, Brech A, Mehlum A, Stenmark H (2003) Hrs regulates multivesicular body formation via ESCRT recruitment to endosomes. The Journal of cell biology 162:435-442. doi:10.1083/jcb.200302131
5. Behl C (2016) Breaking BAG: The Co-Chaperone BAG3 in Health and Disease. Trends Pharmacol Sci 37:672-688. doi:10.1016/j.tips.2016.04.007
6. Bernhardt R, Matus A (1984) Light and electron microscopic studies of the distribution of microtubule-associated protein 2 in rat brain: a difference between dendritic and axonal cytoskeletons. The Journal of comparative neurology 226:203-221. doi:10.1002/cne.902260205
7. Binder LI, Frankfurter A, Kim H, Caceres A, Payne MR, Rebhun LI (1984) Heterogeneity of microtubule-associated protein 2 during rat brain development. Proceedings of the National Academy of Sciences of the United States of America 81:5613-5617. doi:10.1073/pnas.81.17.5613
8. Cao YL, Yang YP, Mao CJ, Zhang XQ, Wang CT, Yang J, Lv DJ, Wang F, Hu LF, Liu CF (2017) A role of BAG3 in regulating SNCA/alpha-synuclein clearance via selective macroautophagy. Neurobiology of aging 60:104-115. doi:10.1016/j.neurobiolaging.2017.08.023
9. Carra S, Seguin SJ, Lambert H, Landry J (2008) HspB8 chaperone activity toward poly(Q)-containing proteins depends on its association with Bag3, a stimulator of macroautophagy. The Journal of biological chemistry 283:1437-1444. doi:10.1074/jbc.M706304200
10. Cataldo AM, Peterhoff CM, Troncoso JC, Gomez-Isla T, Hyman BT, Nixon RA (2000) Endocytic pathway abnormalities precede amyloid beta deposition in sporadic Alzheimer's disease and Down syndrome: differential effects of APOE genotype and presenilin mutations. The American journal of pathology 157:277-286. doi:10.1016/s0002-9440(10)64538-5
11. Cerri S, Blandini F (2019) Role of Autophagy in Parkinson's Disease. Curr Med Chem 26:3702-3718. doi:10.2174/0929867325666180226094351
12. Chakraborty D, Felzen V, Hiebel C, Sturner E, Perumal N, Manicam C, Sehn E, Grus F, Wolfrum U, Behl C (2019) Enhanced autophagic-lysosomal activity and increased BAG3-mediated selective macroautophagy as adaptive response of neuronal cells to chronic oxidative stress. Redox Biol 24:101181. doi:10.1016/j.redox.2019.101181
13. Chen JJ, Nathaniel DL, Raghavan P, Nelson M, Tian R, Tse E, Hong JY, See SK, Mok SA, Hein MY, Southworth DR, Grinberg LT, Gestwicki JE, Leonetti MD, Kampmann M (2019) Compromised function of the ESCRT pathway promotes endolysosomal escape of tau seeds and propagation of tau aggregation. The Journal of biological chemistry 294:18952-18966. doi:10.1074/jbc.RA119.009432
14. Chen XQ, Mobley WC (2019) Alzheimer Disease Pathogenesis: Insights From Molecular and Cellular Biology Studies of Oligomeric Abeta and Tau Species. Front Neurosci 13:659. doi:10.3389/fnins.2019.00659

15. Chen Y, Yang LN, Cheng L, Tu S, Guo SJ, Le HY, Xiong Q, Mo R, Li CY, Jeong JS, Jiang L, Blackshaw S, Bi LJ, Zhu H, Tao SC, Ge F (2013) Bcl2-associated athanogene 3 interactome analysis reveals a new role in modulating proteasome activity. Mol Cell Proteomics 12:2804-2819. doi:10.1074/mcp.M112.025882
16. Cherry JD, Olschowka JA, O'Banion MK (2015) Arginase 1+ microglia reduce Aβ plaque deposition during IL-1β-dependent neuroinflammation. Journal of neuroinflammation 12:203-203. doi:10.1186/s12974-015-0411-8
17. Chevallier J, Koop C, Srivastava A, Petrie RJ, Lamarche-Vane N, Presley JF (2009) Rab35 regulates neurite outgrowth and cell shape. FEBS Lett 583:1096-1101. doi:10.1016/j.febslet.2009.03.012
18. Cho JH, Johnson GV (2003) Glycogen synthase kinase 3beta phosphorylates tau at both primed and unprimed sites. Differential impact on microtubule binding. The Journal of biological chemistry 278:187-193. doi:10.1074/jbc.M206236200
19. Clavaguera F, Bolmont T, Crowther RA, Abramowski D, Frank S, Probst A, Fraser G, Stalder AK, Beibel M, Staufenbiel M, Jucker M, Goedert M, Tolnay M (2009) Transmission and spreading of tauopathy in transgenic mouse brain. Nature cell biology 11:909-913. doi:10.1038/ncb1901
20. Doong H, Rizzo K, Fang S, Kulpa V, Weissman AM, Kohn EC (2003) CAIR-1/BAG-3 abrogates heat shock protein-70 chaperone complex-mediated protein degradation: accumulation of poly-ubiquitinated Hsp90 client proteins. The Journal of biological chemistry 278:28490-28500. doi:10.1074/jbc.M209682200
21. Feldman AM, Gordon J, Wang J, Song J, Zhang XQ, Myers VD, Tilley DG, Gao E, Hoffman NE, Tomar D, Madesh M, Rabinowitz J, Koch WJ, Su F, Khalili K, Cheung JY (2016) BAG3 regulates contractility and Ca(2+) homeostasis in adult mouse ventricular myocytes. Journal of molecular and cellular cardiology 92:10-20. doi:10.1016/j.yjmcc.2016.01.015
22. Frankel EB, Audhya A (2018) ESCRT-dependent cargo sorting at multivesicular endosomes. Semin Cell Dev Biol 74:4-10. doi:10.1016/j.semcdb.2017.08.020
23. Fu H, Possenti A, Freer R, Nakano Y, Hernandez Villegas NC, Tang M, Cauhy PVM, Lassus BA, Chen S, Fowler SL, Figueroa HY, Huey ED, Johnson GVW, Vendruscolo M, Duff KE (2019) A tau homeostasis signature is linked with the cellular and regional vulnerability of excitatory neurons to tau pathology. Nature neuroscience 22:47-56. doi:10.1038/s41593-018-0298-7
24. Fuchs E, Haas AK, Spooner RA, Yoshimura S, Lord JM, Barr FA (2007) Specific Rab GTPase-activating proteins define the Shiga toxin and epidermal growth factor uptake pathways. The Journal of cell biology 177:1133-1143. doi:10.1083/jcb.200612068
25. Fuchs M, Luthold C, Guilbert SM, Varlet AA, Lambert H, Jette A, Elowe S, Landry J, Lavoie JN (2015) A Role for the Chaperone Complex BAG3-HSPB8 in Actin Dynamics, Spindle Orientation and Proper Chromosome Segregation during Mitosis. PLoS genetics 11:e1005582. doi:10.1371/journal.pgen.1005582
26. Fuchs M, Poirier DJ, Seguin SJ, Lambert H, Carra S, Charette SJ, Landry J (2009) Identification of the key structural motifs involved in HspB8/HspB6-Bag3 interaction. Biochem J 425:245-255. doi:10.1042/BJ20090907
27. Gamerdinger M, Hajieva P, Kaya AM, Wolfrum U, Hartl FU, Behl C (2009) Protein quality control during aging involves recruitment of the macroautophagy pathway by BAG3. The EMBO journal 28:889-901. doi:10.1038/emboj.2009.29
28. Henne WM, Buchkovich NJ, Emr SD (2011) The ESCRT pathway. Dev Cell 21:77-91. doi:10.1016/j.devcel.2011.05.015
29. Hipp MS, Kasturi P, Hartl FU (2019) The proteostasis network and its decline in ageing. Nature reviews Molecular cell biology 20:421-435. doi:10.1038/s41580-019-0101-y

30. Hishiya A, Kitazawa T, Takayama S (2010) BAG3 and Hsc70 interact with actin capping protein CapZ to maintain myofibrillar integrity under mechanical stress. Circulation research 107:1220-1231. doi:10.1161/CIRCRESAHA.110.225649
31. Hsu C, Morohashi Y, Yoshimura S, Manrique-Hoyos N, Jung S, Lauterbach MA, Bakhti M, Gronborg M, Mobius W, Rhee J, Barr FA, Simons M (2010) Regulation of exosome secretion by Rab35 and its GTPase-activating proteins TBC1D10A-C. J Cell Biol 189:223-232. doi:10.1083/jcb.200911018
32. Hu YB, Dammer EB, Ren RJ, Wang G (2015) The endosomal-lysosomal system: from acidification and cargo sorting to neurodegeneration. Transl Neurodegener 4:18. doi:10.1186/s40035-015-0041-1
33. Hunt CA, Schenker LJ, Kennedy MB (1996) PSD-95 is associated with the postsynaptic density and not with the presynaptic membrane at forebrain synapses. The Journal of neuroscience : the official journal of the Society for Neuroscience 16:1380-1388
34. Jadhav S, Avila J, Scholl M, Kovacs GG, Kovari E, Skrabana R, Evans LD, Kontsekova E, Malawska B, de Silva R, Buee L, Zilka N (2019) A walk through tau therapeutic strategies. Acta Neuropathol Commun 7:22. doi:10.1186/s40478-019-0664-z
35. Ji C, Tang M, Johnson GVW (2017) Assessing the degradation of tau in primary neurons: The role of autophagy. Methods Cell Biol 141:229-244. doi:10.1016/bs.mcb.2017.06.011
36. Ji C, Tang M, Zeidler C, Hohfeld J, Johnson GV (2019) BAG3 and SYNPO (synaptopodin) facilitate phospho-MAPT/Tau degradation via autophagy in neuronal processes. Autophagy 15:1199-1213. doi:10.1080/15548627.2019.1580096
37. Jiang Y, Sato Y, Im E, Berg M, Bordi M, Darji S, Kumar A, Mohan PS, Bandyopadhyay U, Diaz A, Cuervo AM, Nixon RA (2019) Lysosomal Dysfunction in Down Syndrome Is APP-Dependent and Mediated by APP-betaCTF (C99). The Journal of neuroscience : the official journal of the Society for Neuroscience 39:5255-5268. doi:10.1523/JNEUROSCI.0578-19.2019
38. Jicha GA, Bowser R, Kazam IG, Davies P (1997) Alz-50 and MC-1, a new monoclonal antibody raised to paired helical filaments, recognize conformational epitopes on recombinant tau. Journal of neuroscience research 48:128-132. doi:10.1002/(sici)1097-4547(19970415)48:2<128::aid-jnr5>3.0.co;2-e
39. Johnson GV, Seubert P, Cox TM, Motter R, Brown JP, Galasko D (1997) The tau protein in human cerebrospinal fluid in Alzheimer's disease consists of proteolytically derived fragments. Journal of neurochemistry 68:430-433. doi:10.1046/j.1471-4159.1997.68010430.x
40. Kathage B, Gehlert S, Ulbricht A, Ludecke L, Tapia VE, Orfanos Z, Wenzel D, Bloch W, Volkmer R, Fleischmann BK, Furst DO, Hohfeld J (2017) The cochaperone BAG3 coordinates protein synthesis and autophagy under mechanical strain through spatial regulation of mTORC1. Biochim Biophys Acta Mol Cell Res 1864:62-75. doi:10.1016/j.bbamcr.2016.10.007
41. Kimura T, Yamashita S, Fukuda T, Park JM, Murayama M, Mizoroki T, Yoshiike Y, Sahara N, Takashima A (2007) Hyperphosphorylated tau in parahippocampal cortex impairs place learning in aged mice expressing wild-type human tau. The EMBO journal 26:5143-5152. doi:10.1038/sj.emboj.7601917
42. Kiyota T, Yamamoto M, Schroder B, Jacobsen MT, Swan RJ, Lambert MP, Klein WL, Gendelman HE, Ransohoff RM, Ikezu T (2009) AAV1/2-mediated CNS gene delivery of dominant-negative CCL2 mutant suppresses gliosis, beta-amyloidosis, and learning impairment of APP/PS1 mice. Mol Ther 17:803-809. doi:10.1038/mt.2009.44
43. Klaips CL, Jayaraj GG, Hartl FU (2018) Pathways of cellular proteostasis in aging and disease. The Journal of cell biology 217:51-63. doi:10.1083/jcb.201709072
44. Klimek C, Kathage B, Wordehoff J, Hohfeld J (2017) BAG3-mediated proteostasis at a glance. Journal of cell science 130:2781-2788. doi:10.1242/jcs.203679

45. Klinkert K, Echard A (2016) Rab35 GTPase: A Central Regulator of Phosphoinositides and F-actin in Endocytic Recycling and Beyond. Traffic 17:1063-1077. doi:10.1111/tra.12422
46. Kobayashi H, Etoh K, Marubashi S, Ohbayashi N, Fukuda M (2015) Measurement of Rab35 activity with the GTP-Rab35 trapper RBD35. Methods Mol Biol 1298:207-216. doi:10.1007/978-1-4939-2569-8_18
47. Kouranti I, Sachse M, Arouche N, Goud B, Echard A (2006) Rab35 regulates an endocytic recycling pathway essential for the terminal steps of cytokinesis. Current biology : CB 16:1719-1725. doi:10.1016/j.cub.2006.07.020
48. Kruger L, Mandelkow EM (2016) Tau neurotoxicity and rescue in animal models of human Tauopathies. Current opinion in neurobiology 36:52-58. doi:10.1016/j.conb.2015.09.004
49. Kurtishi A, Rosen B, Patil KS, Alves GW, Moller SG (2019) Cellular Proteostasis in Neurodegeneration. Molecular neurobiology 56:3676-3689. doi:10.1007/s12035-018-1334-z
50. Lasagna-Reeves CA, Castillo-Carranza DL, Sengupta U, Sarmiento J, Troncoso J, Jackson GR, Kayed R (2012) Identification of oligomers at early stages of tau aggregation in Alzheimer's disease. FASEB journal : official publication of the Federation of American Societies for Experimental Biology 26:1946-1959. doi:10.1096/fj.11-199851
51. Lei Z, Brizzee C, Johnson GV (2015) BAG3 facilitates the clearance of endogenous tau in primary neurons. Neurobiology of aging 36:241-248. doi:10.1016/j.neurobiolaging.2014.08.012
52. Li Q, Liu Y, Sun M (2017) Autophagy and Alzheimer's Disease. Cellular and molecular neurobiology 37:377-388. doi:10.1007/s10571-016-0386-8
53. Li X, Colvin T, Rauch JN, Acosta-Alvear D, Kampmann M, Dunyak B, Hann B, Aftab BT, Murnane M, Cho M, Walter P, Weissman JS, Sherman MY, Gestwicki JE (2015) Validation of the Hsp70-Bag3 protein-protein interaction as a potential therapeutic target in cancer. Molecular cancer therapeutics 14:642-648. doi:10.1158/1535-7163.MCT-14-0650
54. Long JM, Holtzman DM (2019) Alzheimer Disease: An Update on Pathobiology and Treatment Strategies. Cell 179:312-339. doi:10.1016/j.cell.2019.09.001
55. Majumder P, Chakrabarti O (2016) ESCRTs and associated proteins in lysosomal fusion with endosomes and autophagosomes. Biochem Cell Biol 94:443-450. doi:10.1139/bcb-2016-0099
56. Makani V, Zhang B, Han H, Yao Y, Lassalas P, Lou K, Paterson I, Lee VM, Trojanowski JQ, Ballatore C, Smith AB, 3rd, Brunden KR (2016) Evaluation of the brain-penetrant microtubule-stabilizing agent, dictyostatin, in the PS19 tau transgenic mouse model of tauopathy. Acta Neuropathol Commun 4:106. doi:10.1186/s40478-016-0378-4
57. Mignogna ML, D'Adamo P (2018) Critical importance of RAB proteins for synaptic function. Small GTPases 9:145-157. doi:10.1080/21541248.2016.1277001
58. Nixon RA (2020) The aging lysosome: An essential catalyst for late-onset neurodegenerative diseases. Biochim Biophys Acta Proteins Proteom 1868:140443. doi:10.1016/j.bbapap.2020.140443
59. Nottingham RM, Pfeffer SR (2009) Defining the boundaries: Rab GEFs and GAPs. Proceedings of the National Academy of Sciences of the United States of America 106:14185-14186. doi:10.1073/pnas.0907725106
60. Peng I, Binder LI, Black MM (1986) Biochemical and immunological analyses of cytoskeletal domains of neurons. The Journal of cell biology 102:252-262. doi:10.1083/jcb.102.1.252
61. Pensalfini A, Kim S, Subbanna S, Bleiwas C, Goulbourne CN, Stavrides PH, Jiang Y, Lee JH, Darji S, Pawlik M, Huo C, Peddy J, Berg MJ, Smiley JF, Basavarajappa BS, Nixon RA (2020) Endosomal Dysfunction Induced by Directly Overactivating Rab5 Recapitulates Prodromal and Neurodegenerative Features of Alzheimer's Disease. Cell reports 33:108420. doi:10.1016/j.celrep.2020.108420

62. Rauch JN, Gestwicki JE (2014) Binding of human nucleotide exchange factors to heat shock protein 70 (Hsp70) generates functionally distinct complexes in vitro. The Journal of biological chemistry 289:1402-1414. doi:10.1074/jbc.M113.521997
63. Rivera-Molina FE, Novick PJ (2009) A Rab GAP cascade defines the boundary between two Rab GTPases on the secretory pathway. Proceedings of the National Academy of Sciences of the United States of America 106:14408-14413. doi:10.1073/pnas.0906536106
64. Rosenzweig R, Nillegoda NB, Mayer MP, Bukau B (2019) The Hsp70 chaperone network. Nature reviews Molecular cell biology 20:665-680. doi:10.1038/s41580-019-0133-3
65. Sheehan P, Waites CL (2019) Coordination of synaptic vesicle trafficking and turnover by the Rab35 signaling network. Small GTPases 10:54-63. doi:10.1080/21541248.2016.1270392
66. Sheehan P, Zhu M, Beskow A, Vollmer C, Waites CL (2016) Activity-Dependent Degradation of Synaptic Vesicle Proteins Requires Rab35 and the ESCRT Pathway. The Journal of neuroscience : the official journal of the Society for Neuroscience 36:8668-8686. doi:10.1523/JNEUROSCI.0725-16.2016
67. Skibinski G, Parkinson NJ, Brown JM, Chakrabarti L, Lloyd SL, Hummerich H, Nielsen JE, Hodges JR, Spillantini MG, Thusgaard T, Brandner S, Brun A, Rossor MN, Gade A, Johannsen P, Sorensen SA, Gydesen S, Fisher EM, Collinge J (2005) Mutations in the endosomal ESCRTIII-complex subunit CHMP2B in frontotemporal dementia. Nature genetics 37:806-808. doi:10.1038/ng1609
68. Sondermann H, Scheufler C, Schneider C, Hohfeld J, Hartl FU, Moarefi I (2001) Structure of a Bag/Hsc70 complex: convergent functional evolution of Hsp70 nucleotide exchange factors. Science 291:1553-1557. doi:10.1126/science.1057268
69. Sturner E, Behl C (2017) The Role of the Multifunctional BAG3 Protein in Cellular Protein Quality Control and in Disease. Frontiers in molecular neuroscience 10:177. doi:10.3389/fnmol.2017.00177
70. Suzuki M, Iwasaki M, Sugio A, Hishiya A, Tanaka R, Endo T, Takayama S, Saito T (2011) BAG3 (BCL2-associated athanogene 3) interacts with MMP-2 to positively regulate invasion by ovarian carcinoma cells. Cancer letters 303:65-71. doi:10.1016/j.canlet.2011.01.019
71. Tang M, Ji C, Pallo S, Rahman I, Johnson GVW (2018) Nrf2 mediates the expression of BAG3 and autophagy cargo adaptor proteins and tau clearance in an age-dependent manner. Neurobiology of aging 63:128-139. doi:10.1016/j.neurobiolaging.2017.12.001
72. Vaz-Silva J, Gomes P, Jin Q, Zhu M, Zhuravleva V, Quintremil S, Meira T, Silva J, Dioli C, Soares-Cunha C, Daskalakis NP, Sousa N, Sotiropoulos I, Waites CL (2018) Endolysosomal degradation of Tau and its role in glucocorticoid-driven hippocampal malfunction. The EMBO journal 37. doi:10.15252/embj.201899084
73. Wenzel EM, Schultz SW, Schink KO, Pedersen NM, Nahse V, Carlson A, Brech A, Stenmark H, Raiborg C (2018) Concerted ESCRT and clathrin recruitment waves define the timing and morphology of intraluminal vesicle formation. Nature communications 9:2932. doi:10.1038/s41467-018-05345-8
74. Wesseling H, Mair W, Kumar M, Schlaffner CN, Tang S, Beerepoot P, Fatou B, Guise AJ, Cheng L, Takeda S, Muntel J, Rotunno MS, Dujardin S, Davies P, Kosik KS, Miller BL, Berretta S, Hedreen JC, Grinberg LT, Seeley WW, Hyman BT, Steen H, Steen JA (2020) Tau PTM Profiles Identify Patient Heterogeneity and Stages of Alzheimer's Disease. Cell 183:1699-1713 e1613. doi:10.1016/j.cell.2020.10.029
75. Winckler B, Faundez V, Maday S, Cai Q, Guimas Almeida C, Zhang H (2018) The Endolysosomal System and Proteostasis: From Development to Degeneration. The Journal of neuroscience : the official journal of the Society for Neuroscience 38:9364-9374. doi:10.1523/JNEUROSCI.1665-18.2018

76. Xu Z, Graham K, Foote M, Liang F, Rizkallah R, Hurt M, Wang Y, Wu Y, Zhou Y (2013) 14-3-3 protein targets misfolded chaperone-associated proteins to aggresomes. Journal of cell science 126:4173-4186. doi:10.1242/jcs.126102
77. Yamashita Y, Kojima K, Tsukahara T, Agawa H, Yamada K, Amano Y, Kurotori N, Tanaka N, Sugamura K, Takeshita T (2008) Ubiquitin-independent binding of Hrs mediates endosomal sorting of the interleukin-2 receptor beta-chain. Journal of cell science 121:1727-1738. doi:10.1242/jcs.024455
78. Yin Y, Gao D, Wang Y, Wang ZH, Wang X, Ye J, Wu D, Fang L, Pi G, Yang Y, Wang XC, Lu C, Ye K, Wang JZ (2016) Tau accumulation induces synaptic impairment and memory deficit by calcineurin-mediated inactivation of nuclear CaMKIV/CREB signaling. Proceedings of the National Academy of Sciences of the United States of America 113:E3773-3781. doi:10.1073/pnas.1604519113
79. Yoshiyama Y, Higuchi M, Zhang B, Huang SM, Iwata N, Saido TC, Maeda J, Suhara T, Trojanowski JQ, Lee VM (2007) Synapse loss and microglial activation precede tangles in a P301S tauopathy mouse model. Neuron 53:337-351. doi:10.1016/j.neuron.2007.01.010
80. Zhang B, Carroll J, Trojanowski JQ, Yao Y, Iba M, Potuzak JS, Hogan AM, Xie SX, Ballatore C, Smith AB, 3rd, Lee VM, Brunden KR (2012) The microtubule-stabilizing agent, epothilone D, reduces axonal dysfunction, neurotoxicity, cognitive deficits, and Alzheimer-like pathology in an interventional study with aged tau transgenic mice. The Journal of neuroscience : the official journal of the Society for Neuroscience 32:3601-3611. doi:10.1523/JNEUROSCI.4922-11.2012
81. Zhen Y, Stenmark H (2015) Cellular functions of Rab GTPases at a glance. Journal of cell science 128:3171-3176. doi:10.1242/jcs.166074
82. Zhou J, Chow HM, Liu Y, Wu D, Shi M, Li J, Wen L, Gao Y, Chen G, Zhuang K, Lin H, Zhang G, Xie W, Li H, Leng L, Wang M, Zheng N, Sun H, Zhao Y, Zhang Y, Xue M, Huang TY, Bu G, Xu H, Yuan Z, Herrup K, Zhang J (2020) Cyclin-Dependent Kinase 5-Dependent BAG3 Degradation Modulates Synaptic Protein Turnover. Biol Psychiatry 87:756-769. doi:10.1016/j.biopsych.2019.11.013

Figure legends

Fig 1 BAG3 interacts with proteins of the endocytosis pathway. Rat cortical neurons were transduced with lentivirus expressing scrambled (Scr) or shBAG3 shRNA. Neurons were subsequently collected, BAG3 was immunoprecipitated, and mass spectrometry was used to identify BAG3-interacting proteins (neurons transduced with shBAG3 were used as a control for non-specific interactions). (a) KEGG enrichment analysis of the BAG3 associated proteins (PSM(Scr/shBAG3)>3) was generated using STRING online software (http://string-db.org). FDR threshold was set at -log10>1. (b) STRING was used to visualize predicted protein-protein interactions for the identified BAG3 associated proteins based on confidence. Line thickness indicates the strength of data support (http://string-db.org). Prominent clusters of the proteins that co-immunoprecipitated with BAG3 represented proteins involved in vacuolar processes and chaperone/co-chaperone proteins, both of which are associated with endocytosis. Nodes directly linked to vacuolar processes are labeled in red, and nodes that are related to chaperone/co-chaperone proteins are labeled in green. Rab35 did not co-immunoprecipitate with BAG3 but is included with the node being surrounded by a dotted line. BAG3 and TBC1D10B are in red font. FDR, false discovery rate. KEGG, Kyoto Encyclopedia of Genes and Genomes.

Fig 2 BAG3 associates with TBC1D10B in neurons. (a) Rat cortical neuron lysates were immunoprecipitated with a TBC1D10B antibody and immunoblotted for BAG3. The same amount of non-immune rabbit IgG was used to verify the specificity of the immunoprecipitation. An indicated fraction of cell lysate was used as input control. Immunoprecipitates were probed for TBC1D10B, BAG3, and Rab35. GAPDH was used as a loading control for the input lanes. The positions at which molecular weight markers (kDa) migrated are indicated at the left. Vertical dashed lines indicate that intervening lanes were removed, however, all images were from the same blot and exposure. (b) Immunostaining of brain sections from an 8 month old male wild type C57Bl/6 mouse (which had been intrahippocampally injected with AAV9 control virus for another study) shows colocalization of BAG3 (green) and TBC1D10B (red). The sample was counterstained with Hoechst 33342 to visualize the nuclei. The CA1 region of the hippocampus was imaged. Scale bars, 20μm. (c-f) Neurons were co-immunostained for BAG3 (red) and TBC1D10B (green). Overlap of BAG3 with TBC1D10B puncta was observed in the neurites (d) and soma (f). (e and g) The corresponding line scans are shown at right for neurites of d and line of f. Arrowheads indicate areas of overlap. Scale bar: 10 μm.

Fig 3 HSP70 facilitates the association of BAG3 with TBC1D10B at the BAG domain. (a) BAG3 null HEK293TN cells were transiently transfected with FLAG-TBC1D10B together with empty vector (Control), wild type BAG3 (WT BAG3), or different form of BAG3 mutant including, WAWA BAG3, GPG BAG3, or L462P BAG3. Cell lysates were collected at 48 hours post-transfection for all studies. The cell lysates were immunoprecipitated with FLAG tag antibody, followed by blotting for BAG3 and FLAG. Immunoprecipitates were probed for FLAG and BAG3. (b) BAG3 null HEK293TN cells were transiently transfected with V5-HSP70 together with wild type BAG3 (WT) or L462P BAG3 (L462P). Cell lysates were immunoprecipitated with V5 tag antibody, followed by blotting for BAG3 and V5. (c) HEK293TN cells were transiently transfected with FLAG-TBC1D10B together with an empty vector (Control) or V5-HSP70. Cell lysates were immunoprecipitated with FLAG tag, followed by blotting for endogenous BAG3, as well as FLAG-TBC1D10B and V5-HSP70. (d) HEK293TN cells were transient co-expressed with FLAG-TBC1D10B together with an empty vector or V5-HSP70. Cells were treated with 10 μM YM01 or DMSO (vehicle control) at 24 hours post-transfection. Cells were collected 48 hours post-transfection and immunoprecipitated with FLAG tag antibody, followed by blotting for BAG3, V5, and FLAG. (e) BAG3 null HEK293TN cells were transient co-expressed with V5-HSP70 and FLAG-TBC1D10B. Cells were immunoprecipitated with FLAG tag antibody, followed by blotting for V5 and FLAG. Results of different exposure times for the same blot were separate with a vertical dotted line. The same amount of control IgG was used to verify the specificity of the immunoprecipitation. 4% fraction of cell lysate was used as input control. In all panels, the positions at which molecular weight markers (kDa) migrated are indicated at the left, and GAPDH was used as a loading control for the input lanes.

Fig 4 BAG3 associates with TBC1D10B to regulate the Rab35 activity. (a) Rat cortical neurons were transduced with lentivirus expressing shBAG3 or a scrambled (Scr) version. Cell lysates were immunoprecipitated with an anti-TBC1D10B antibody and immunoblotted for BAG3, TBC1D10B, and Rab35. An 8% fraction of cell lysate was used as input control. (b) Rat cortical neurons were transduced with lentivirus expressing scrambled (Scr) or shBAG3 shRNA. Rab35 activity was examined by incubation of cell lysates with purified GST or GST-RBD35, followed by precipitation with glutathione beads [46]. The precipitated samples were blotted for Rab35 and GST. 4% of the cell lysate was used as input control. (c) BAG3 null HEK293TN cells were transiently transfected with Myc-Rab35 together with empty vector (Control), wild type BAG3 (WT BAG3) or L462P BAG3. Rab35 activity was examined by pull-down with GST-RBD35, as described in B. The precipitated samples were blot for Rab35 and GST. 1.2% of the cell lysate was used as input control. (d) Rat cortical neurons were transduced with lentivirus expressing

scrambled (Scr), shBAG3, shTBC1D10B, or both shBAG3 and shTBC1D10B shRNAs. Rab35 activity was examined by pull-down with GST-RBD35. Arrow indicates the GST-RBD35 fusion protein; **, GST-RBD35 degradation products, *, GST protein. In all panels, the positions at which molecular weight markers (kDa) migrated are indicated at the left, and GAPDH was used as a loading control for the input lanes.

Fig 5 BAG3 cooperates with TBC1D10B to regulate tau levels in neurons. (a) Rat cortical neurons were transduced with lentivirus expressing scrambled (Scr) or shTBC1D10B shRNA. Cell lysates were immunoblotted for TBC1D10B, p-Ser262 tau, p-Ser396/404 tau, and p-Thr231 tau. GAPDH is used as a loading control. (b) Quantifications of the level of phosphorylated tau in TBC1D10B knockdown neurons. Data are shown as mean ± SEM. Statistical analysis was performed using the student t-test. **, $P<0.01$. N=3 for each group. (c-d) Rat cortical neurons were transduced with lentivirus expressing scrambled (Scr) or shBAG3 or both shBAG3 and shTBC1D10B shRNAs. Cell lysates were either immunoblotted for BAG3 and TBC1D10B for validating the knockdown (C) or p-Ser262, tau p-Ser396/404 tau, and p-Thr231 tau (d). (e) Quantifications of the level of phosphorylated tau in D. Data are shown as mean ± SEM. Statistical analysis was performed using the student t-test. **, $P<0.01$. N=3 for each group. Vertical dotted lines indicate that intervening lanes were removed, however, all images were from the same blot and exposure. The positions at which molecular weight markers (kDa) migrated are indicated at the left for the immunoblots in a, c and d.

Fig 6. BAG3 interacts with TBC1D10B to regulate the tau sorting into the endocytic pathway through the ESCRT system. (a) Rat cortical neurons were transduced with lentivirus expressing scrambled (Scr), shBAG3, shTBC1D10B or both shBAG3 and shTBC1D10B shRNAs. Neurons were co-immunostained for CHMP2B (red) and p-Ser396/404 (green). Overlap of CHMP2B with p-Ser396/404 puncta was observed in the neurites. The corresponding line scans are shown below for neurites. Arrowheads indicate areas of overlap. Scale bar: 5 μm. (b) Quantification of the colocalization between CHMP2B and p-Ser396/404 based on volume. (c) Quantification of colocalization of CHMP2B and p-Ser396/404 using Mander's coefficient. Ten neurites from at least 6 different cells were used for analysis. Statistical analysis was performed using One-way ANOVA. Data were presented as Mean±SD. *, $P<0.05$, **, $P<0.01$.

Fig 7. BAG3 and TBC1D10B regulate the mobility of Hrs and its interaction with Rab35. (a-f) Rat cortical neurons that were transduced with lentivirus expressing scrambled (Scr) or shBAG3 shRNAs were co-immunostained for Rab35(Green) and Hrs (Red). Overlap of Rab35 with Hrs puncta was observed in the soma (a) and neurites (d). Scale bars, 10 μm. The corresponding line

scans are shown at the bottom for A or right for D. Arrowheads indicate areas of overlap. (b, e) Quantification of the colocalization between Rab35 and Hrs based on volume. (c, f) Quantification of colocalization of Rab35 and Hrs using Mander's coefficient. Twelve neurites from 6 different neurons from each group were used for analysis. Statistical analysis was performed using One-way ANOVA. Data were presented as Mean±SD. *, P<0.05, **, P<0.01. (g) BAG3 null HEK293TN cells were transfected with BAG3 WT (+BAG3) or empty vector (BAG3 KO), RFP-Hrs, and GFP-Rab35. Live-cell imaging was done at 36 hours post-transfection in conventional mode at a frame rate of 0.1 Hz for 10 minutes. g1 and g2, are representative snapshots of HEKS with or without BAG3. g1', g1'' and g2', g2'' are 3D kymographs of g1 and g2. The white color indicates the co-localized region of Rab35 and Hrs over time. Scale bars, 20um. (h) The graph shows the track distance of Hrs puncta in 10 minutes. The distance of the track was binned every 0.1 μm. The percentage of events is defined as the percentage of tracks of Hrs in a certain distance range in one cell. At least 10 cells from each group were analyzed. ($p < 0.01$, Kolmogorov-Smirnov test). (i) The graph shows the average Mander's coefficient of Rab35 and Hrs in each cell over time in BAG3+ and BAG3-/- group (Mean±SD). n=12. **, P<0.01. (j) BAG3 null HEK293TN cells were transfected with Myc-Rab35 and with/without BAG3 and TBC1D10B. The cell lysates were immunoprecipitated with Myc tag antibody and immunoblotted for Hrs and Myc. Four percent of the lysates were used for input control. (k-m) BAG3 null HEK293TN cells stably expressing tau were transfected with Myc-Rab35 together with empty vector(Control), wild type BAG3(BAG3 WT), or different mutant forms of BAG3 including, WAWA BAG3, GPG BAG3, and L462P BAG3. (k) Cell lysates were collected at 48 hours post-transfection and immunoblotted for total tau, Hrs and BAG3. (l)The graph on the right shows the level of tau was quantified. N=3 for each group. Data are shown as mean ± SEM. Statistical analysis was performed using the student t-test. **, P<0.01. n.s. not significant. (m) Cell lysates were immunoprecipitated with Myc antibody and immunoblotted for Hrs. For immunoblots shown in f, g, and i, GAPDH is used as a loading control. The positions at which molecular weight markers (kDa) migrated are indicated at the left.

Fig 8. Overexpression of BAG3 in P301S mice in the hippocampus reduced the tau levels. Two-month-old P301S mice were intrahippocampally injected with AAV2/9-eGFP as control or AAV2/9-eGFP-hBAG3 (with a FLAG-Myc N terminal tag) for BAG3 overexpression (BAG3 O/E), and animals were collected at 6 months of age. (a) Images of the AAV injected brains were co-immunostained for BAG3 (red) and Myc tag (purple). The immunofluorescence images showed increased levels of BAG3 in the hippocampal region in the BAG3 O/E brain. Scale bars, 200μm. (b) Hippocampal lysates from control and BAG3 O/E brains were immunoblotted for BAG3. GAPDH is used as a loading control. The positions at which molecular weight markers (kDa)

migrated are indicated at the left. (c) The graph shows the level of BAG3 normalized to GAPDH and relative to control. N=4 for control, n=5 for BAG3 O/E, Data are shown as mean ± SEM. Statistical analysis was performed using the student t-test, *P<0.05. (d, e) Hippocampal lysates from control and BAG3 O/E brains were blot for total human tau (HT7 and 5A6). The graphs on the right show the quantitative analysis of tau normalized to GAPDH and relative to control. N=4 for control, n=5 for BAG3 O/E. (f) Representative blots of phosphorylated tau (p-Thr231, p-Ser262, and p-Ser396/Ser404) in the hippocampus lysate of control and BAG3 O/E brains. (g) Quantification of the levels of phosphorylated tau in control and BAG3 O/E hippocampal lysates. Data were normalized to the loading control GAPDH and then compared to controls. N=4 for control, n=5 for BAG3 O/E. (h, i) The immunofluorescence images show phosphorylated tau (p-Ser262 and p-Ser396/Ser404, Green) in the CA1 region of control and BAG3 O/E brains. The graphs on the right show the intensity of fluorescence of the phosphorylated tau relative to controls. Four animals of each group were used for analysis. (j) The immunofluorescence images show oligomeric tau (T22 tau, purple). The graph on the right shows the percentage of T22 positive cells in the CA1 region. Three animals from each group were used for analysis. (k) The immunofluorescence images show the neurofibrillary tangles in CA1 region of control and BAG3 O/E brains with anti-MC1 tau (Green). The graph on the right shows the intensity of fluorescence of the MC1 tau relative to controls. Scale bars, 20μm. Three brains from each group were used for analysis. The samples were counterstained with Hoechst 33342. Data are shown as mean ± SEM. Statistical analysis was performed using the student t-test. *, P<0.05. **, P<0.01.

Fig 9. Overexpression of BAG3 in P301s mice promotes Rab35 mediated recruitment of Hrs and the tau sorting into the endocytic pathway. Two-month-old P301S mice were intrahippocampally injected with AAV2/9-GFP as control or AAV2/9-GFP-hBAG3 (with a FLAG-Myc N terminal tag) as BAG3 overexpression (BAG3 O/E) and collected at 6-month old. (a) The immunofluorescence images show the colocalization of Rab35 (Green) and Hrs (Red) in the CA1 region of the control and BAG3 O/E brain. The dashed lined rectangles show the magnified CA1 areas. (b) Quantification of colocalization of Hrs and Rab35 using Mander's coefficient. (c) Quantification of the colocalization between Rab35 and Hrs based on volume. Three animals from each group were used for analysis. (d) The immunofluorescence images show the colocalization of p-Ser396/404 tau (green) and CHMP2b (red) in the CA1 region of the control and BAG3 O/E brain. The dashed line rectangles show the magnified CA1 areas. (e) Quantification of colocalization of using Mander's coefficient. (f) Quantification of the colocalization between Rab35 and Hrs. All samples were counterstained with Hoechst 33342 (blue) to visualize the nuclei. Scale bars, 20

μm. Three samples from each group were used for analysis. Statistical analysis was performed using the student t-test. *, P<0.05. **, P<0.01.

Fig 10. Overexpression of BAG3 in P301S mice in the hippocampus increased the density of synapses and dendrites. (a) The immunofluorescence images show the dendrites (MAP2 staining(Green)) and postsynaptic compartment (PSD95 staining (Red)). The samples were counterstained with Hoechst 33342 to visualize the nuclei. CA1 region of the hippocampus was imaged. The confocal images were rendered with the surface function using Imaris in the lower right panels. Scale bars, 20μm. (b& c) The graphs show the relative density of MAP2(b) and PSD95(c) in the yellow rectangle area. The density of MAP2 or PSD95 were defined as the volume of fluorescence positive area/total area. Data are shown as mean ± SEM. Statistical analysis was performed using the student t-test. **, P<0.01. Four sections from 4 brains for each group were used for analysis.

Fig 11. BAG3-TBC1D10B-Rab35 signaling axis in regulate ESCRT and endosomal tau clearance. Schematic diagram shows BAG3-TBC1D10B-Rab35 signaling axis in tau clearance. During normal aging, BAG3 level is increasing over time. Increased BAG3 promotes the association of BAG3-HSP70-TBC1D10B, thus the inactivation function of TBC1D10B on Rab35 is prohibited. The activation of Rab35 recruits Hrs, which initiates the ESCRT-mediated endosomal tau clearance. In AD brains, however, this increase of BAG3 may be attenuated, which would release TBC1D10B from the BAG3-HSP70-TBC1D10B complex. The free TBC1D10B would thus be able to inactivate Rab35 and contribute to the accumulation of phosphorylated tau. Overexpression of BAG3 in a tauopathy mouse model decreased tau levels and helped maintain neuronal health.

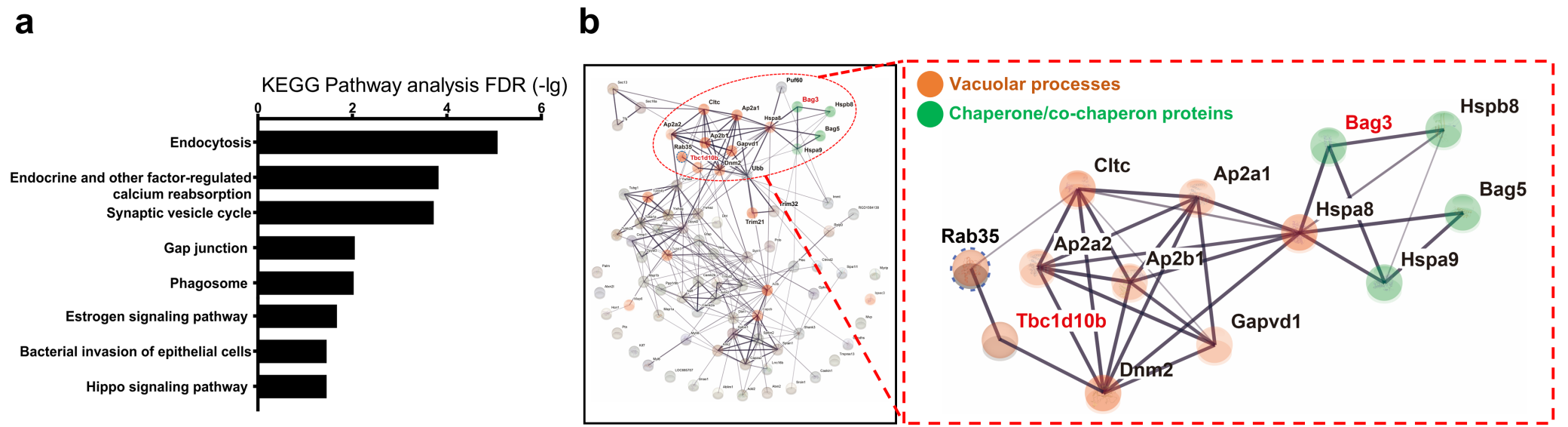
a
KEGG Pathway analysis FDR (-lg)
0
2
4
6
Endocytosis
Endocrine and other factor-regulated calcium reabsorption
Synaptic vesicle cycle
Gap junction
Phagosome
Estrogen signaling pathway
Bacterial invasion of epithelial cells
Hippo signaling pathway
b
Vacuolar processes
Chaperone/co-chaperon proteins
Cltc
Ap2a1
Bag3
Hspb8
Bag5
Hspa8
Rab35
Ap2a2
Ap2b1
Hspa9
Tbc1d10b
Gapvd1
Dnm2

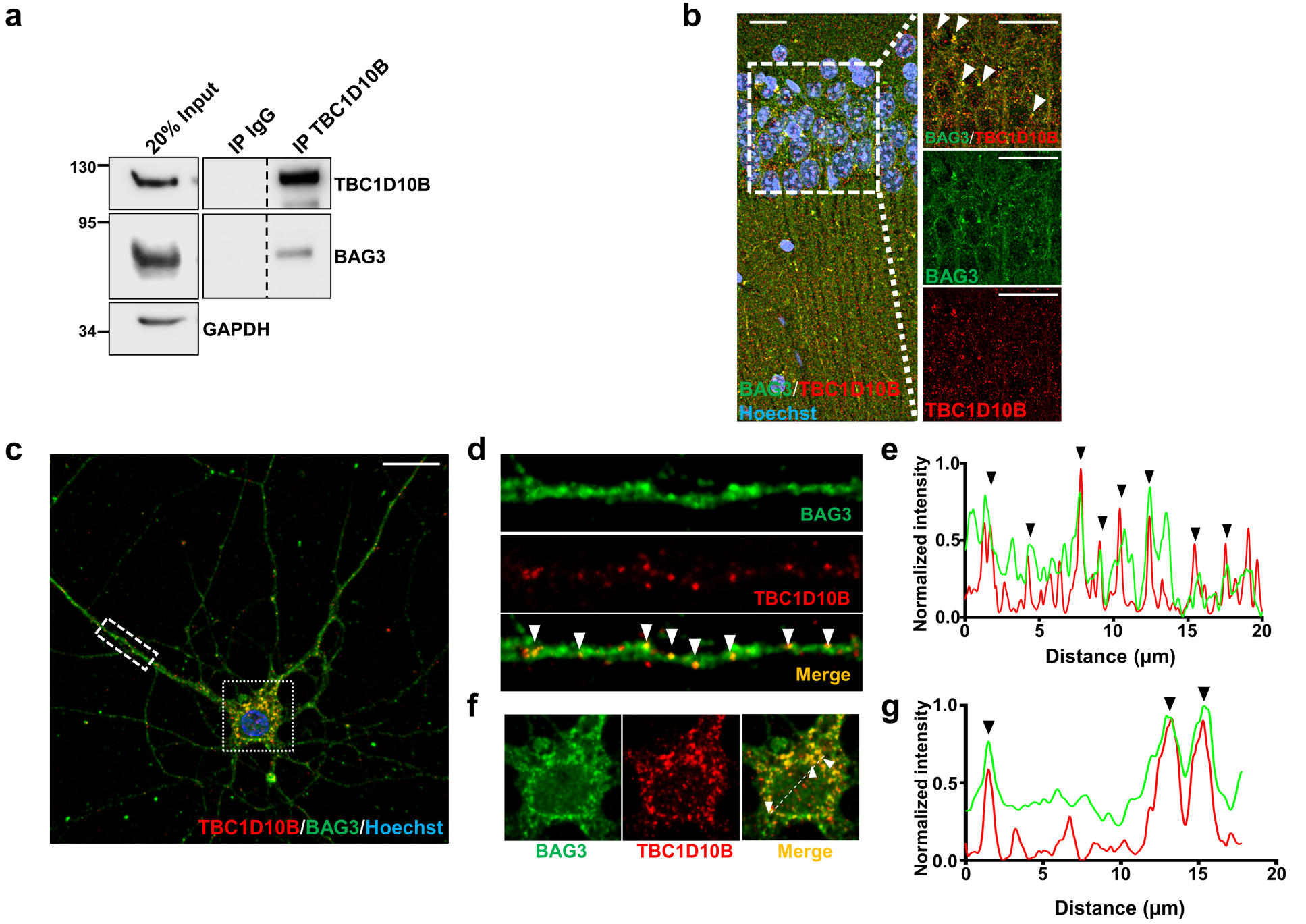
a
20% Input
IP IgG
IP TBC1D10B
130
95
34
TBC1D10B
BAG3
GAPDH
b
BAG3/TBC1D10B
BAG3
TBC1D10B
Hoechst
c
TBC1D10B/BAG3/Hoechst
d
BAG3
TBC1D10B
Merge
e
Normalized intensity
1.0
0.5
0.0
0
5
10
15
20
Distance (μm)
f
BAG3
TBC1D10B
Merge
g
Normalized intensity
1.0
0.5
0.0
0
5
10
15
20
Distance (μm)

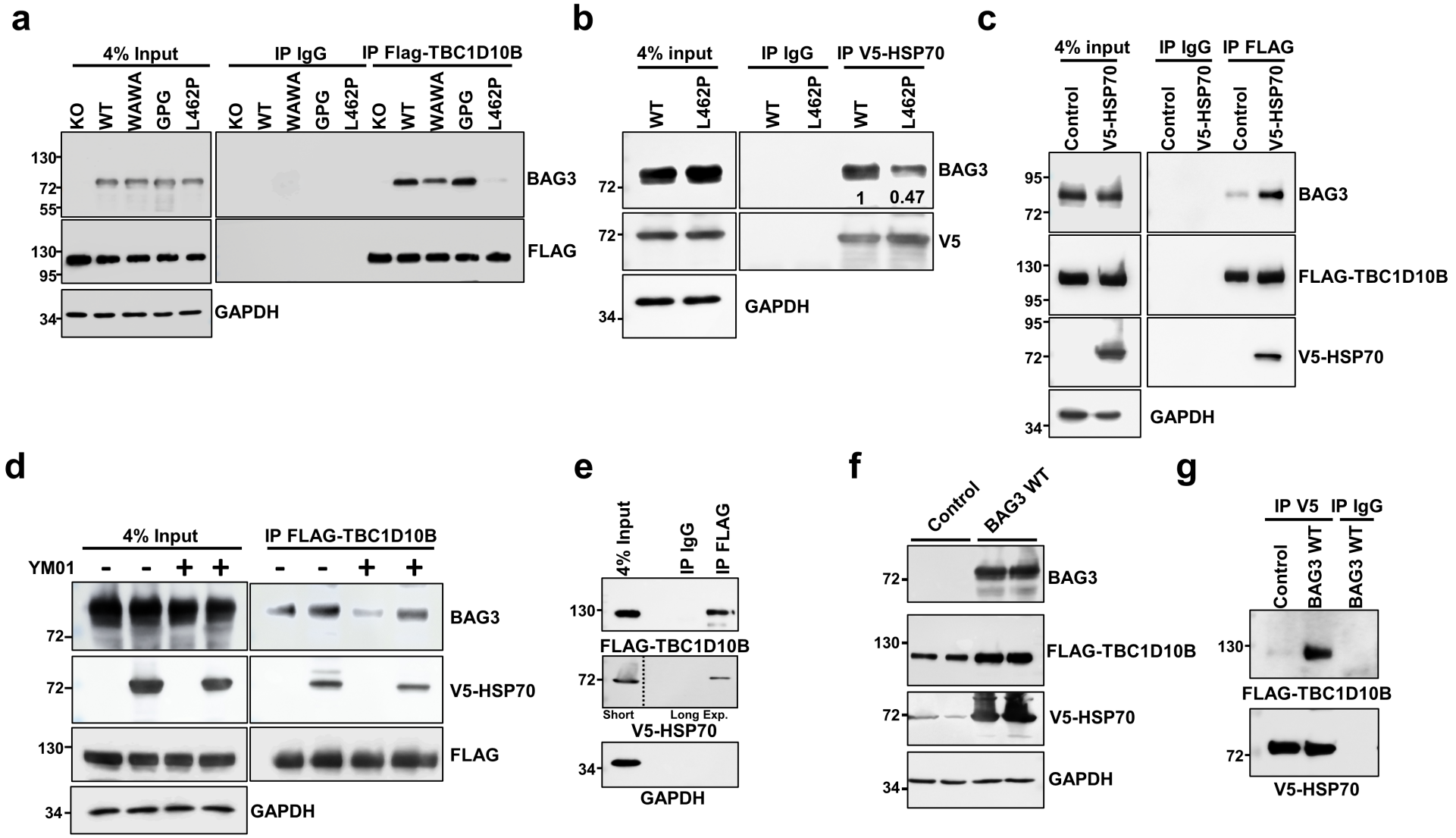
a
4% Input
IP IgG
IP Flag-TBC1D10B
KO
WT
WAWA
GPG
L462P
130
72
55
130
95
34
BAG3
FLAG
GAPDH
b
4% input
IP IgG
IP V5-HSP70
WT
L462P
72
72
34
1
0.47
BAG3
V5
GAPDH
c
4% input
IP IgG
IP FLAG
Control
V5-HSP70
95
72
130
95
95
72
34
BAG3
FLAG-TBC1D10B
V5-HSP70
GAPDH
d
4% Input
IP FLAG-TBC1D10B
YM01
- - + + - - + +
72
72
130
34
BAG3
V5-HSP70
FLAG
GAPDH
e
4% Input
IP IgG
IP FLAG
130
72
34
FLAG-TBC1D10B
Short
Long Exp.
V5-HSP70
GAPDH
f
Control
BAG3 WT
72
130
72
34
BAG3
FLAG-TBC1D10B
V5-HSP70
GAPDH
g
IP V5
IP IgG
Control
BAG3 WT
BAG3 WT
130
72
FLAG-TBC1D10B
V5-HSP70

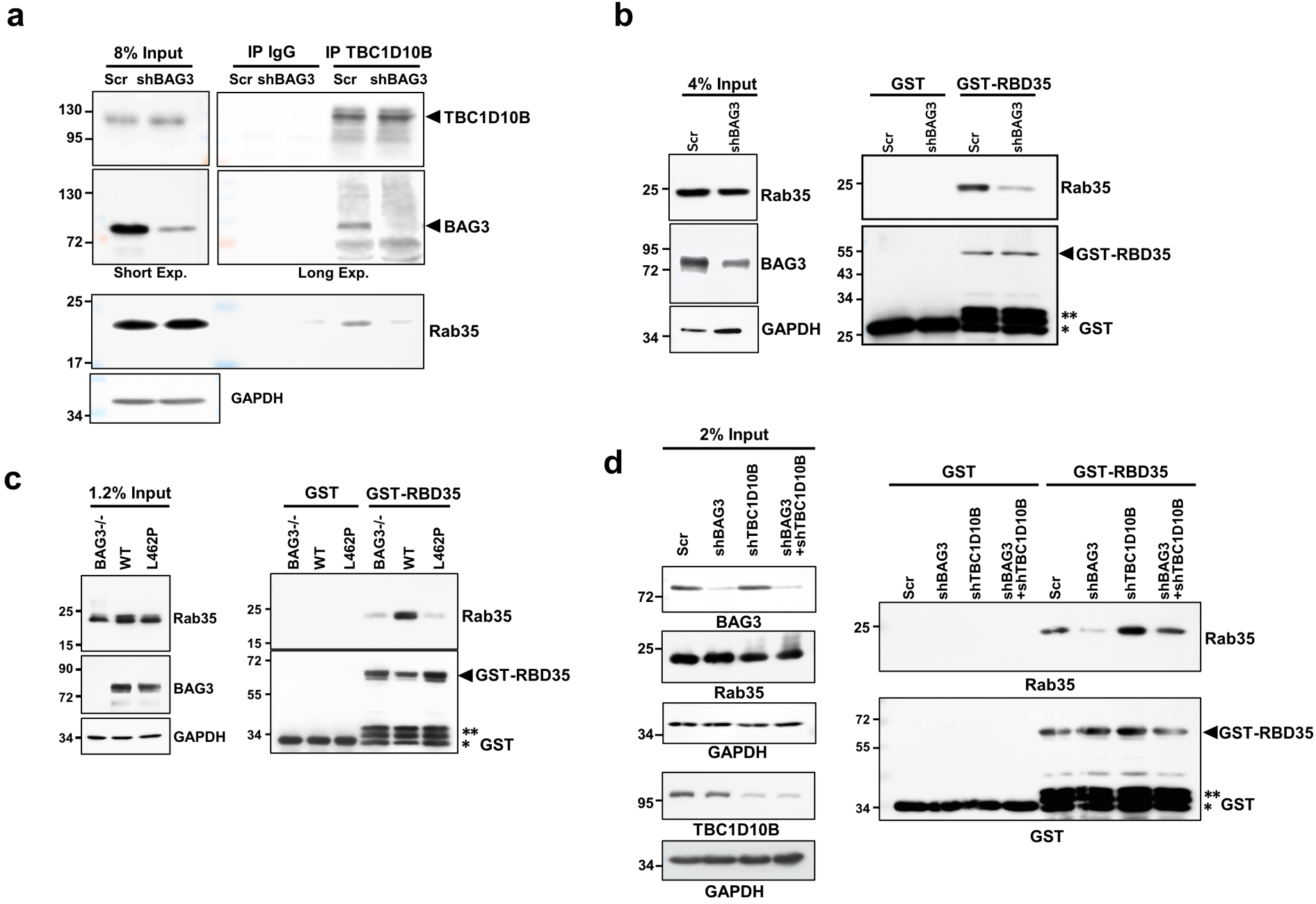
a
8% Input
IP IgG
IP TBC1D10B
Scr shBAG3
Scr shBAG3
Scr shBAG3
130
95
TBC1D10B
130
72
BAG3
Short Exp.
Long Exp.
25
Rab35
17
34
GAPDH
b
4% Input
GST
GST-RBD35
Scr
shBAG3
Scr
shBAG3
25
Rab35
95
72
BAG3
34
GAPDH
25
Rab35
55
43
34
25
GST-RBD35
** GST
c
1.2% Input
GST
GST-RBD35
BAG3-/-
WT
L462P
BAG3-/-
WT
L462P
BAG3-/-
WT
L462P
25
15
Rab35
90
72
BAG3
34
GAPDH
25
15
Rab35
72
55
34
GST-RBD35
** GST
d
2% Input
Scr
shBAG3
shTBC1D10B
shBAG3 +shTBC1D10B
72
BAG3
25
Rab35
34
GAPDH
95
TBC1D10B
34
GAPDH
GST
GST-RBD35
Scr
shBAG3
shTBC1D10B
shBAG3 +shTBC1D10B
Scr
shBAG3
shTBC1D10B
shBAG3 +shTBC1D10B
25
Rab35
Rab35
72
55
34
GST-RBD35
** GST
GST

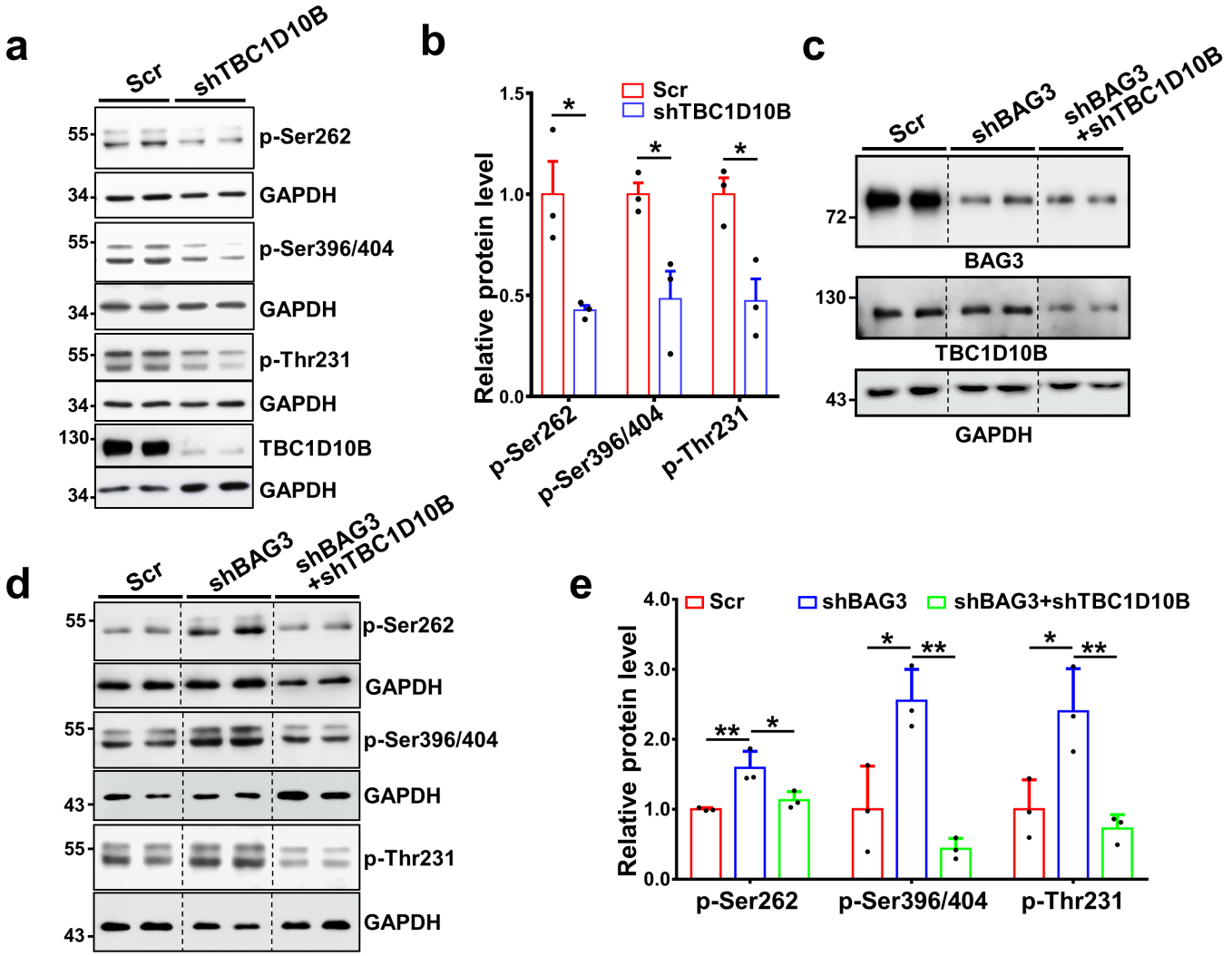

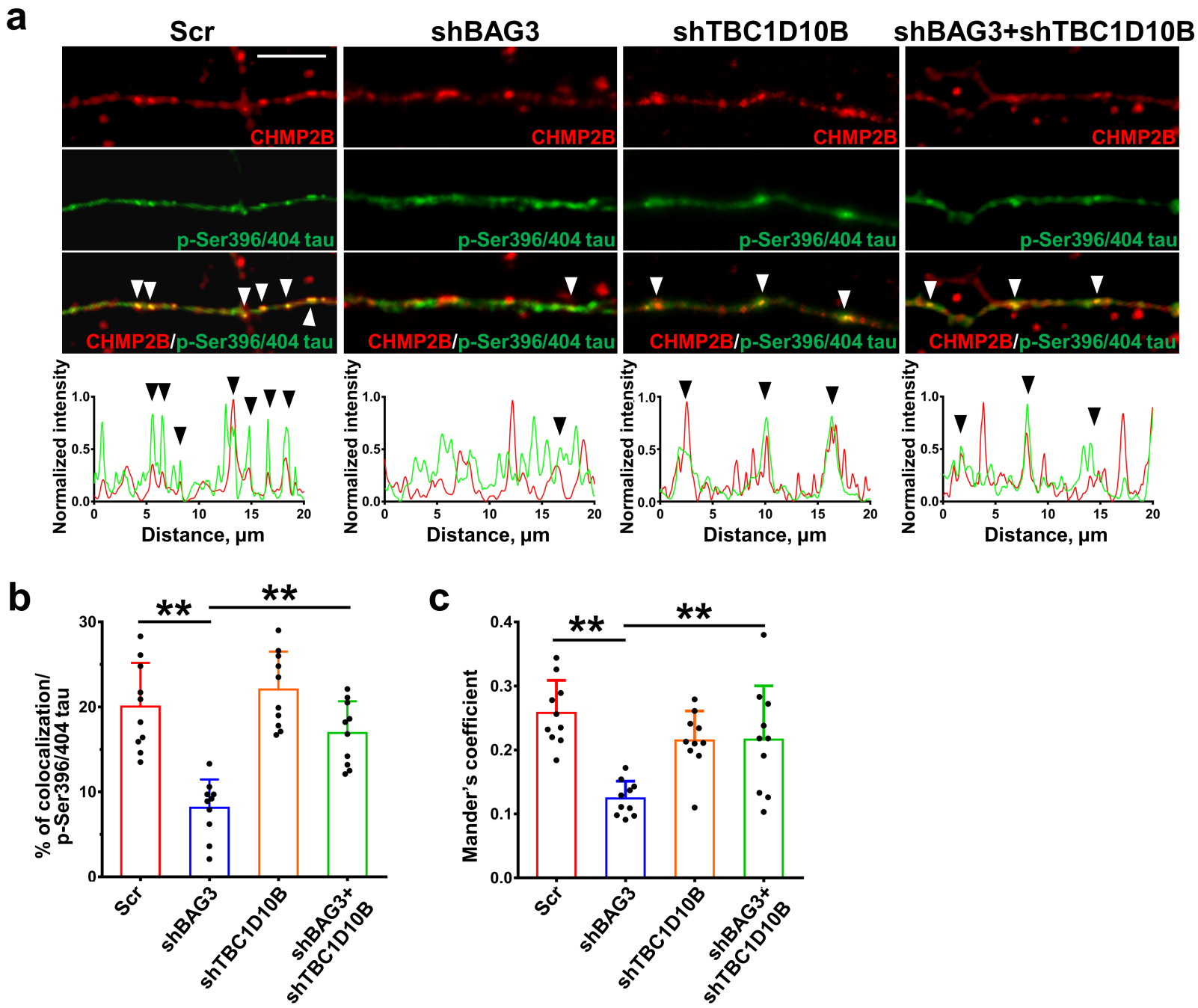
a
Scr
shBAG3
shTBC1D10B
shBAG3+shTBC1D10B
CHMP2B
p-Ser396/404 tau
CHMP2B/p-Ser396/404 tau
Normalized intensity
Distance, μm
b
% of colocalization/ p-Ser396/404 tau
c
Mander's coefficient
Scr
shBAG3
shTBC1D10B
shBAG3+ shTBC1D10B
**

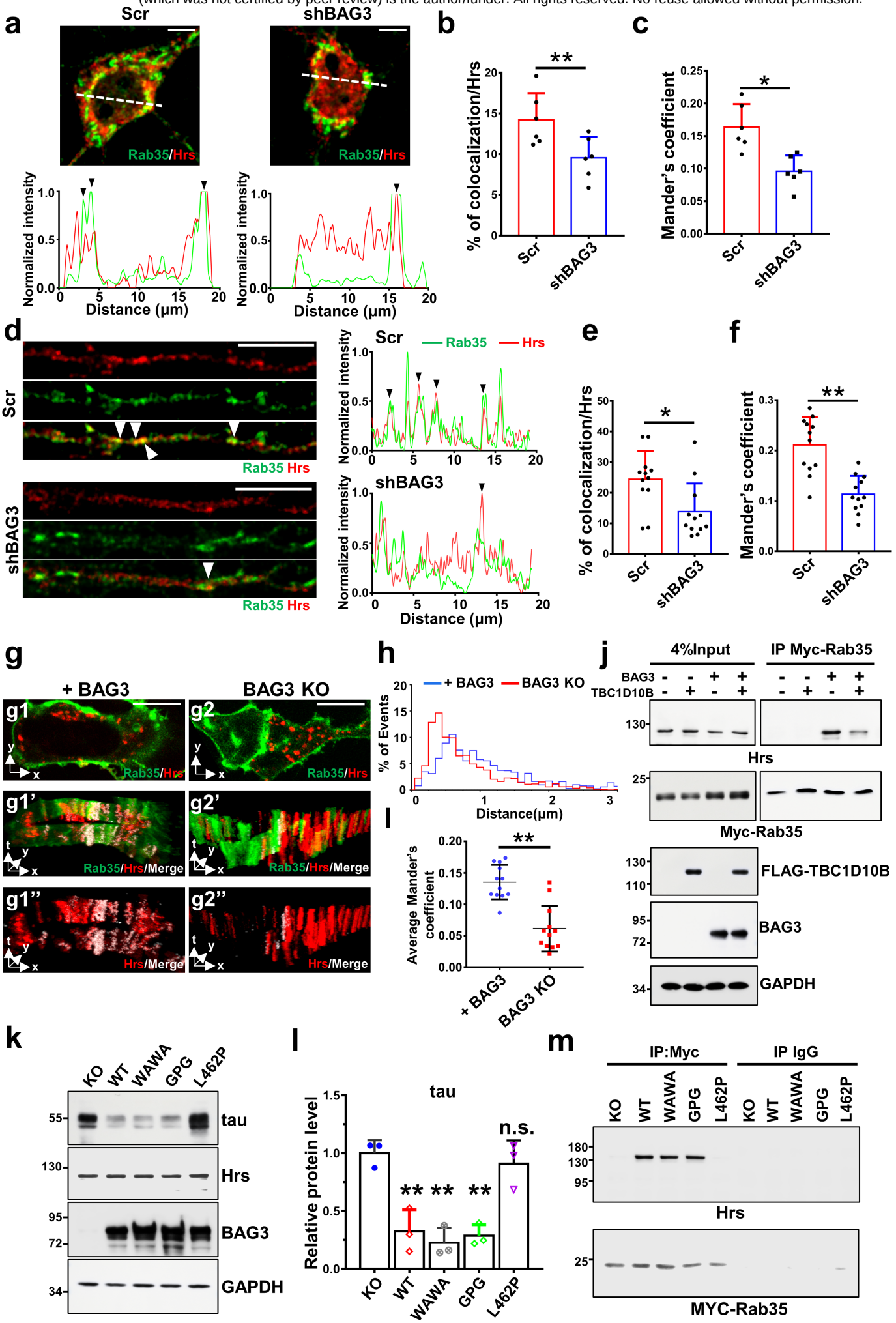

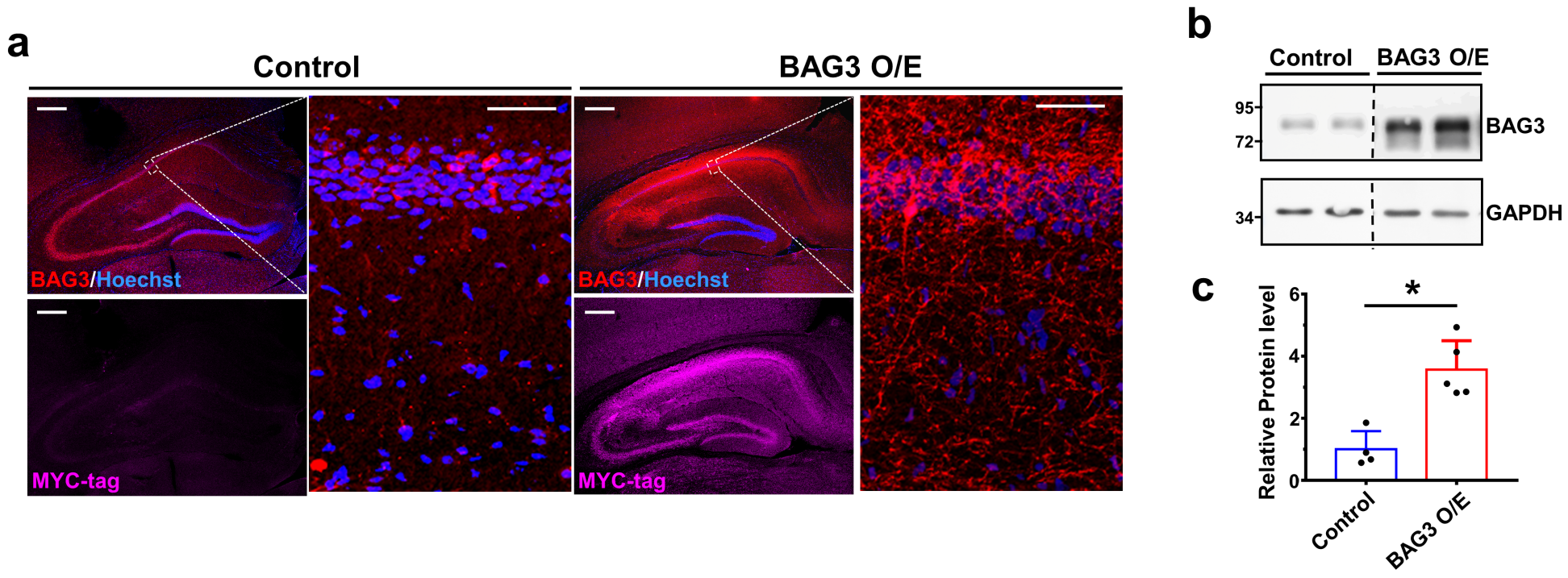
a
Control
BAG3 O/E
BAG3/Hoechst
MYC-tag
BAG3/Hoechst
MYC-tag
b
Control
BAG3 O/E
95
72
BAG3
34
GAPDH
c
Relative Protein level
6
4
2
0
*
Control
BAG3 O/E

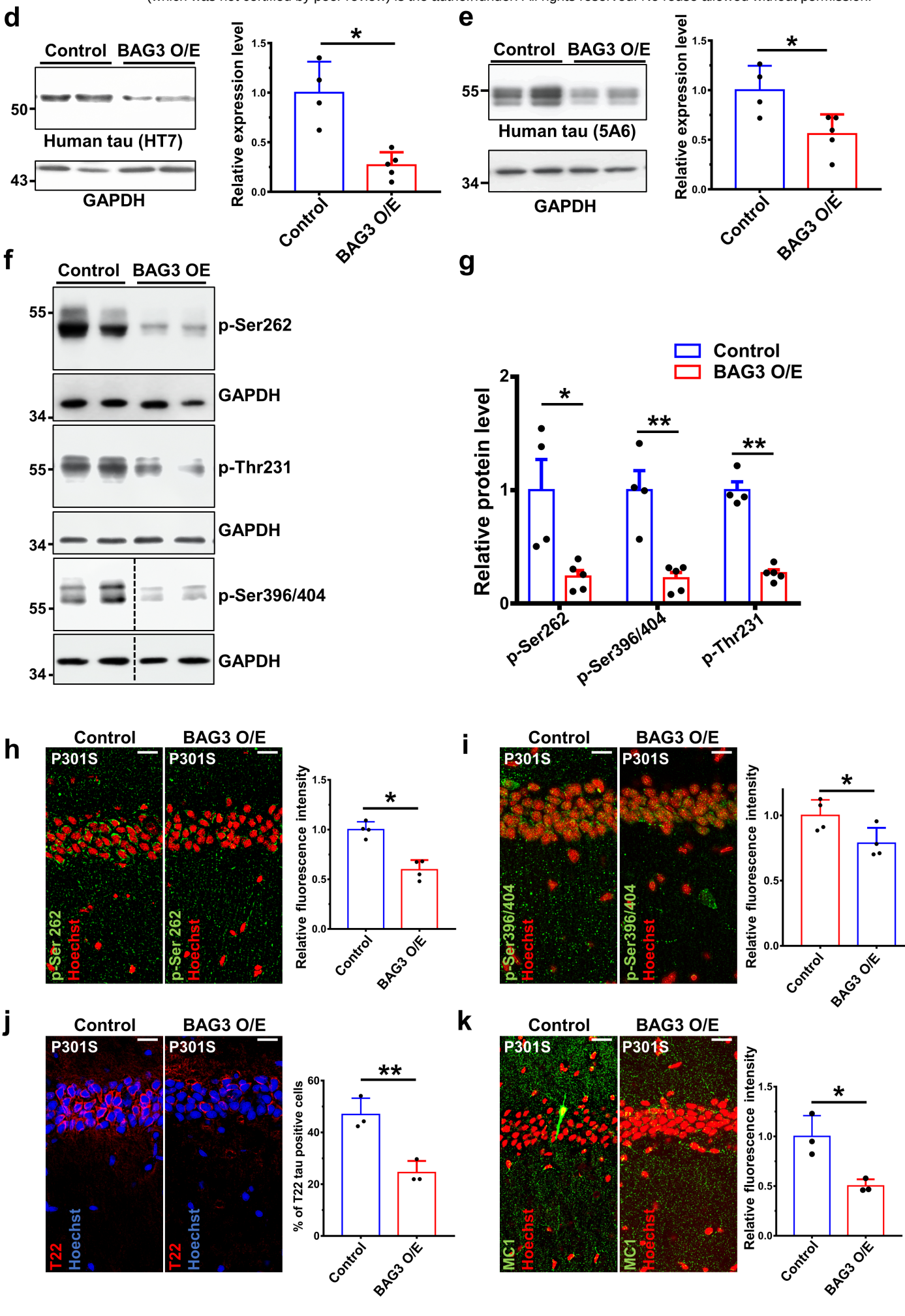

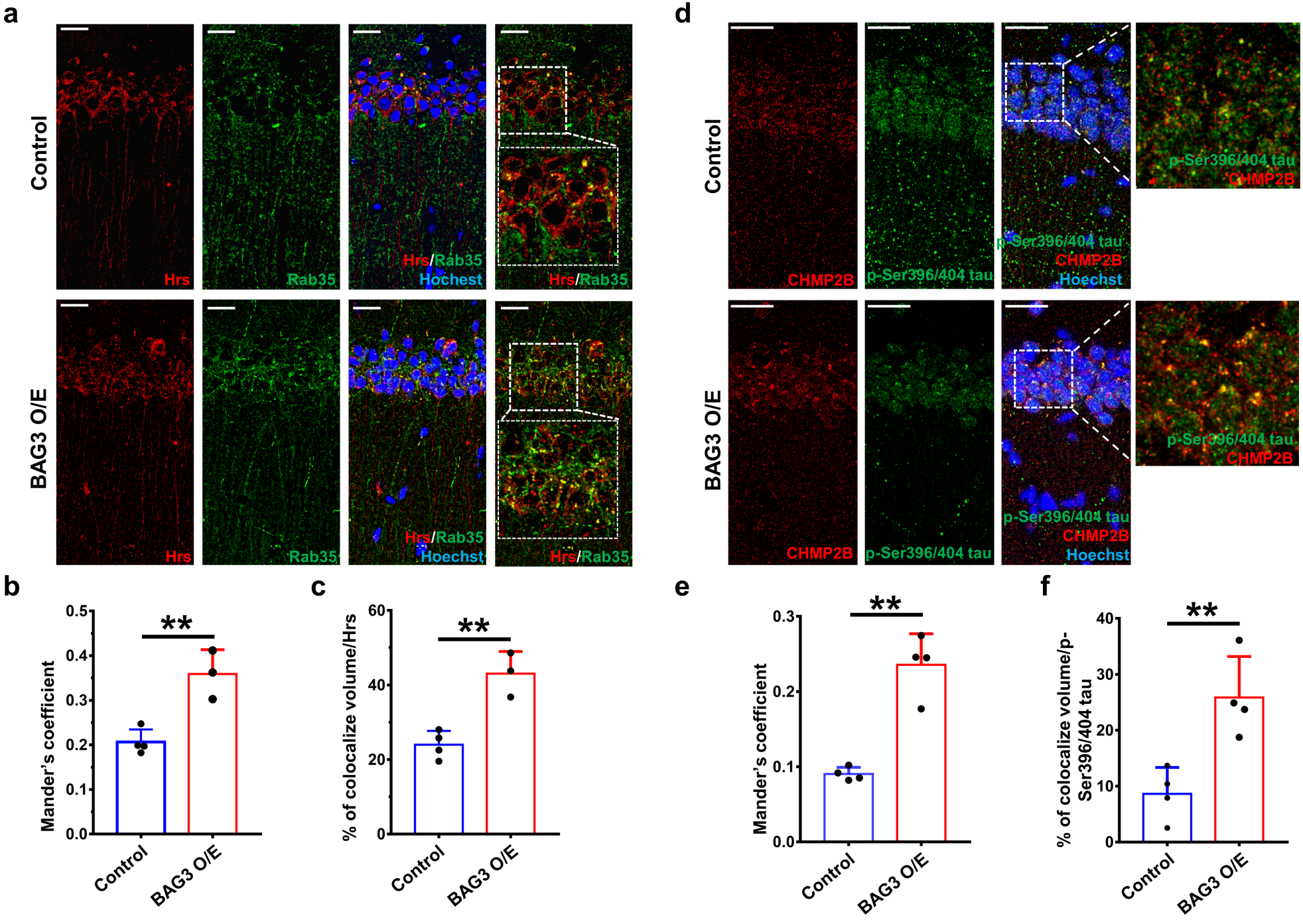
a
Control
BAG3 O/E
Hrs
Rab35
Hrs/Rab35
Hochest
Hrs/Rab35
Hrs
Rab35
Hrs/Rab35
Hoechst
Hrs/Rab35
d
Control
BAG3 O/E
CHMP2B
p-Ser396/404 tau
p-Ser396/404 tau
CHMP2B
Hoechst
p-Ser396/404 tau
CHMP2B
CHMP2B
p-Ser396/404 tau
CHMP2B
Hoechst
p-Ser396/404 tau
CHMP2B
b
Mander's coefficient
0.0
0.1
0.2
0.3
0.4
0.5
**
Control
BAG3 O/E
c
% of colocalize volume/Hrs
0
20
40
60
**
Control
BAG3 O/E
e
Mander's coefficient
0.0
0.1
0.2
0.3
**
Control
BAG3 O/E
f
% of colocalize volume/p-Ser396/404 tau
0
10
20
30
40
**
Control
BAG3 O/E

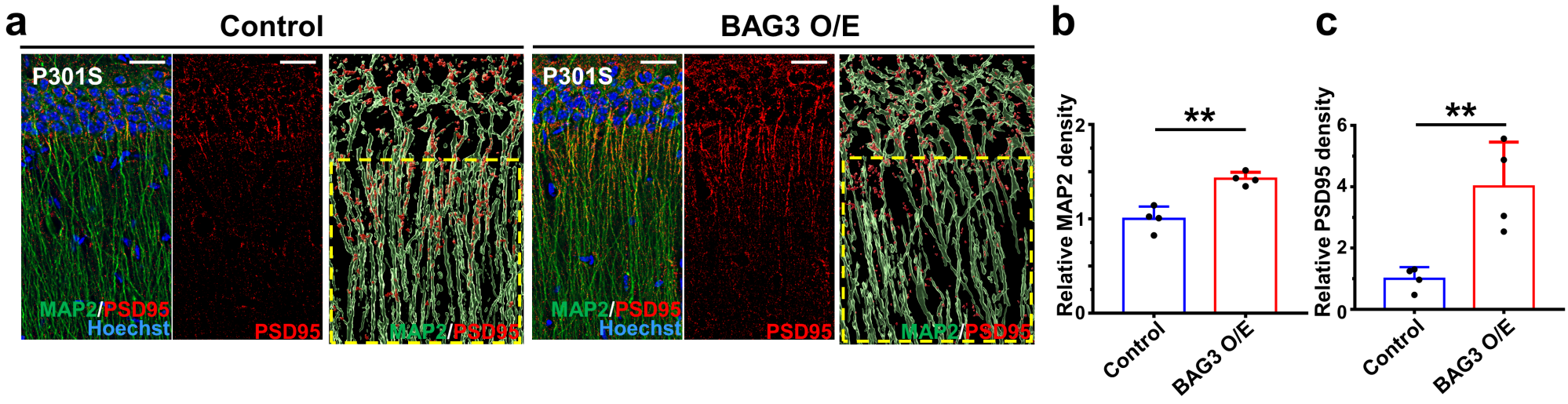
a
Control
BAG3 O/E
P301S
MAP2/PSD95
Hoechst
PSD95
MAP2/PSD95
P301S
MAP2/PSD95
Hoechst
PSD95
MAP2/PSD95
b
Relative MAP2 density
**
Control
BAG3 O/E
c
Relative PSD95 density
**
Control
BAG3 O/E

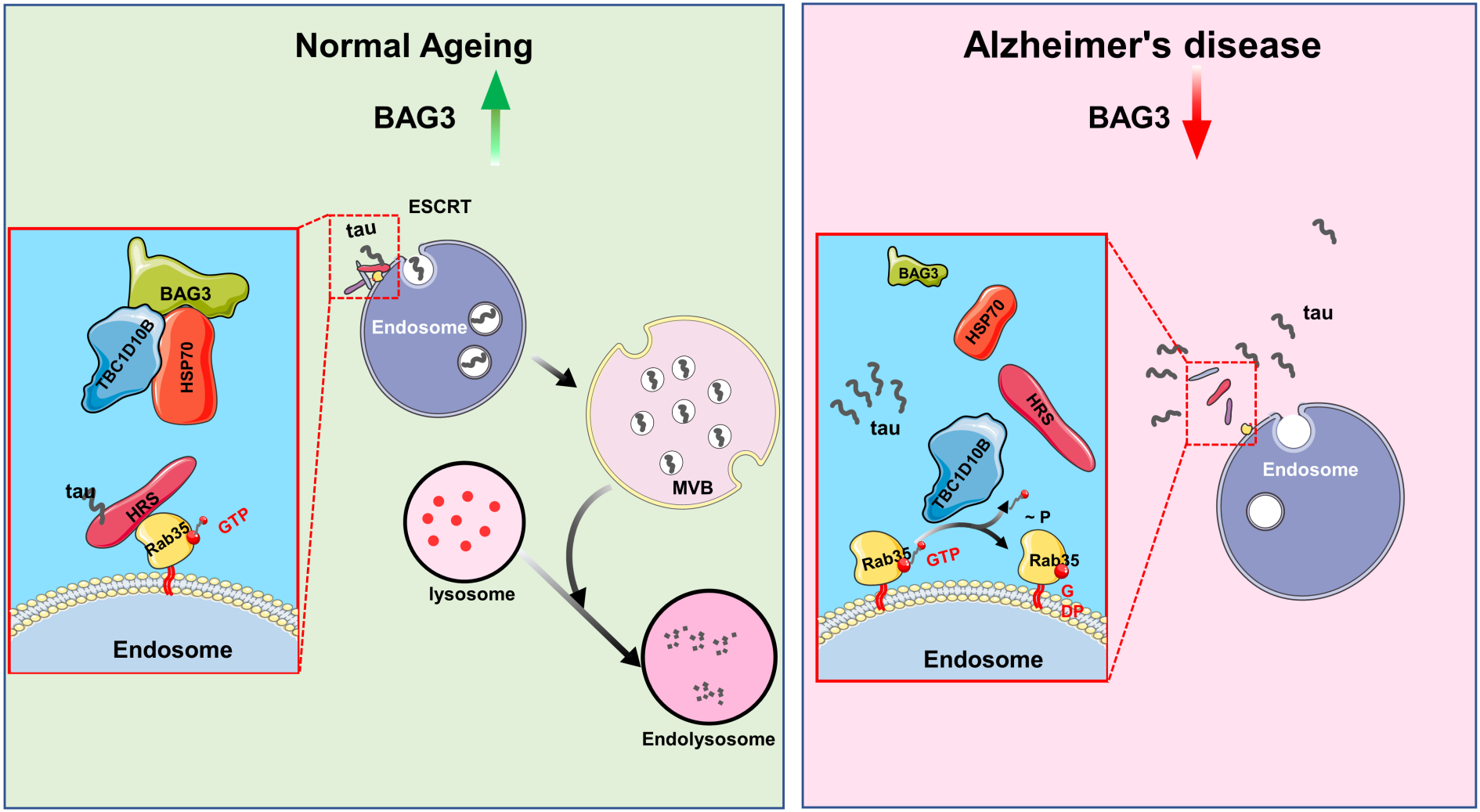
Normal Ageing
BAG3
ESCRT
tau
BAG3
TBC1D10B
HSP70
tau
HRS
Rab35
GTP
Endosome
Endosome
MVB
lysosome
Endolysosome
Alzheimer's disease
BAG3
BAG3
HSP70
tau
HRS
TBC1D10B
~ P
Rab35
GTP
Rab35
G
DP
Endosome
tau
Endosome

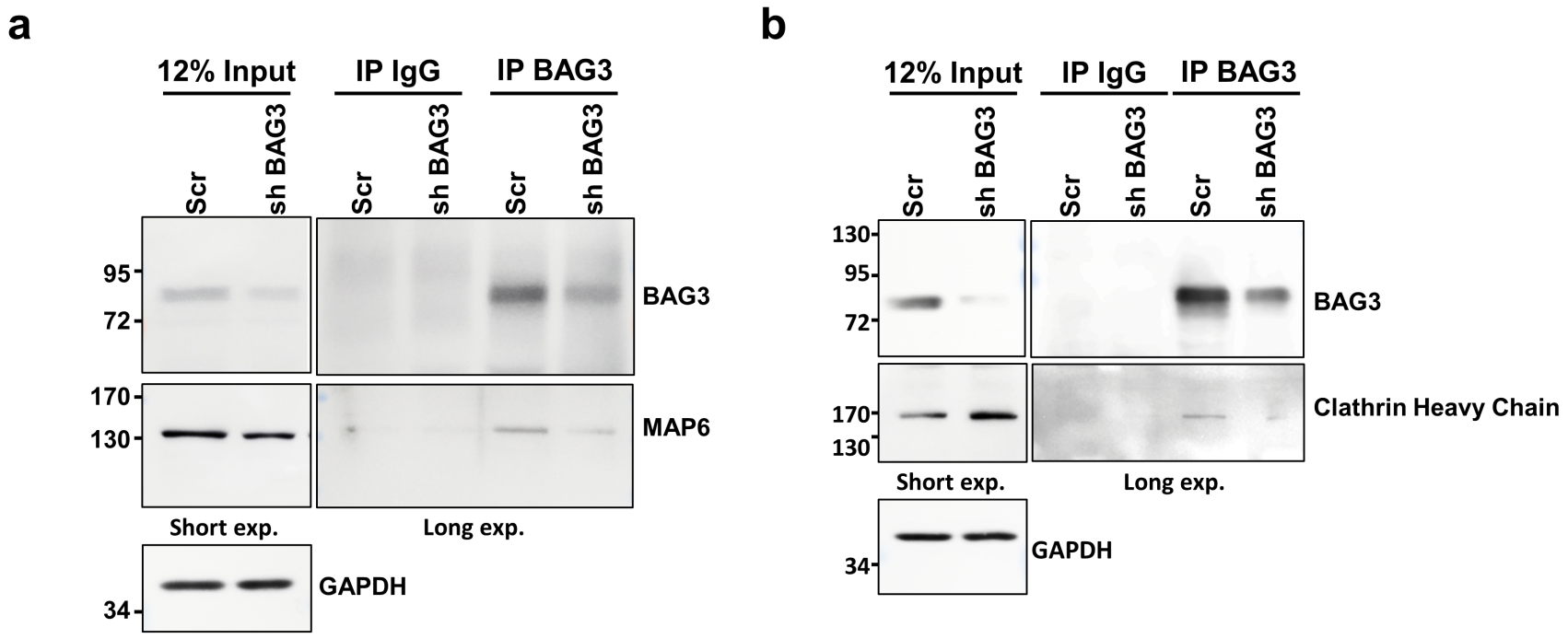

Fig s1. Verification of immunoprecipitation-mass spectrometry data. Cell lysates from rat neurons transduced with lentivirus expressing scrambled or shBAG3 shRNA at DIV16 were collected at DIV 22. MAP6 and clathrin were selected from the list of proteins that co-immunoprecipitated with BAG3 that were identified by mass spectrometry for verification. (a) Cell lysates were immunoprecipitated with an anti-BAG3 antibody and probed for the presence of MAP6. (b) Cell lysates were immunoprecipitated with an anti-BAG3 antibody and probed for the presence of clathrin. The same amount of rabbit IgG was used to verify the specificity of the immunoprecipitation. A fraction of cell lysate was used as input control. GAPDH is used as a loading control. the positions at which molecular weight markers (kDa) migrated are indicated at the left.

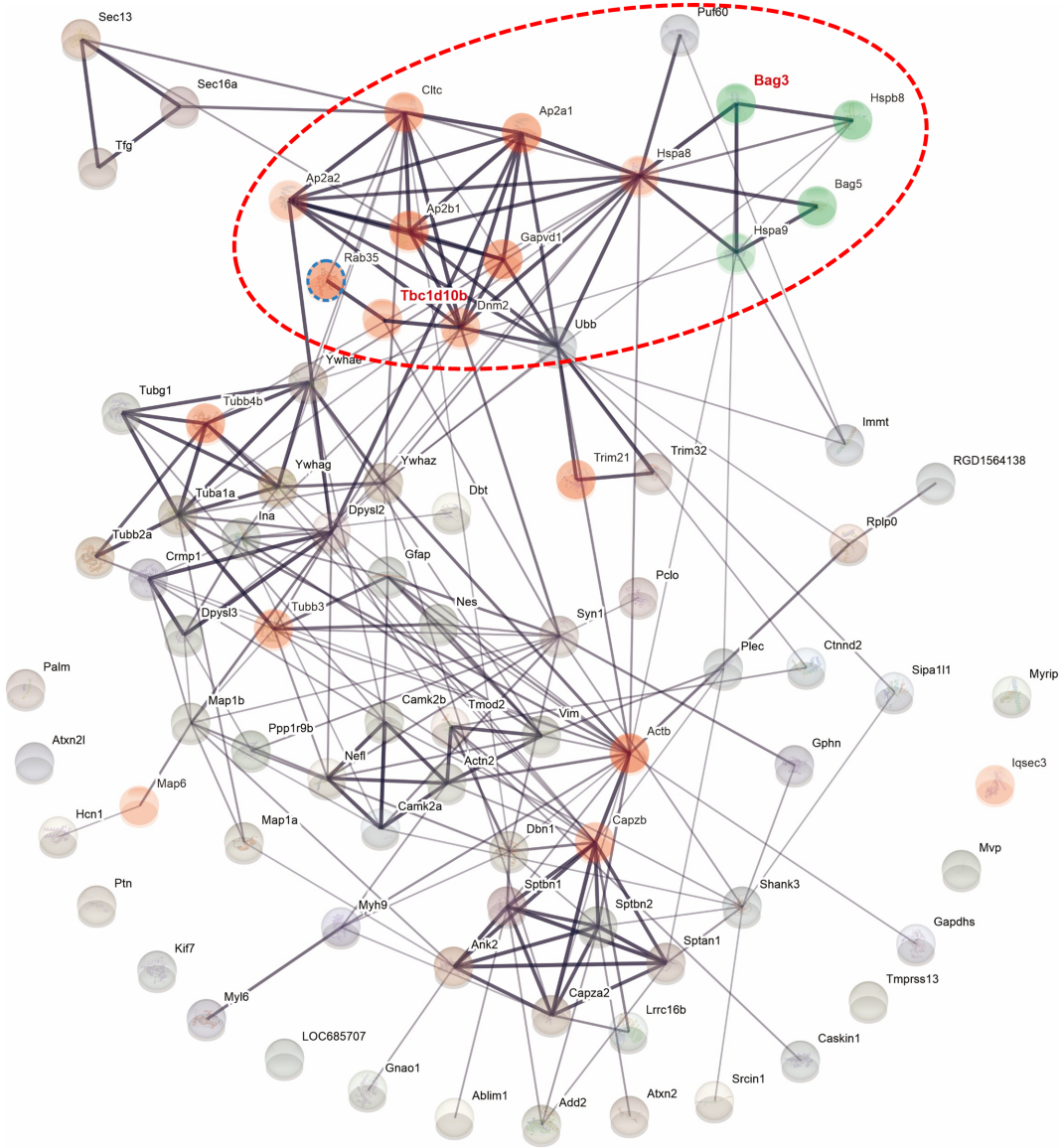

Fig s2. STRING analysis of predicted protein-protein interactions for the identified BAG3 associated proteins based on confidence. STRING analysis reveals that BAG3 associated with a diverse set of proteins which influence on endocytosis. STRING analysis reveals that BAG3 associated with a diverse set of proteins which influence on endocytosis pathway. Magnified image of Fig 1b.

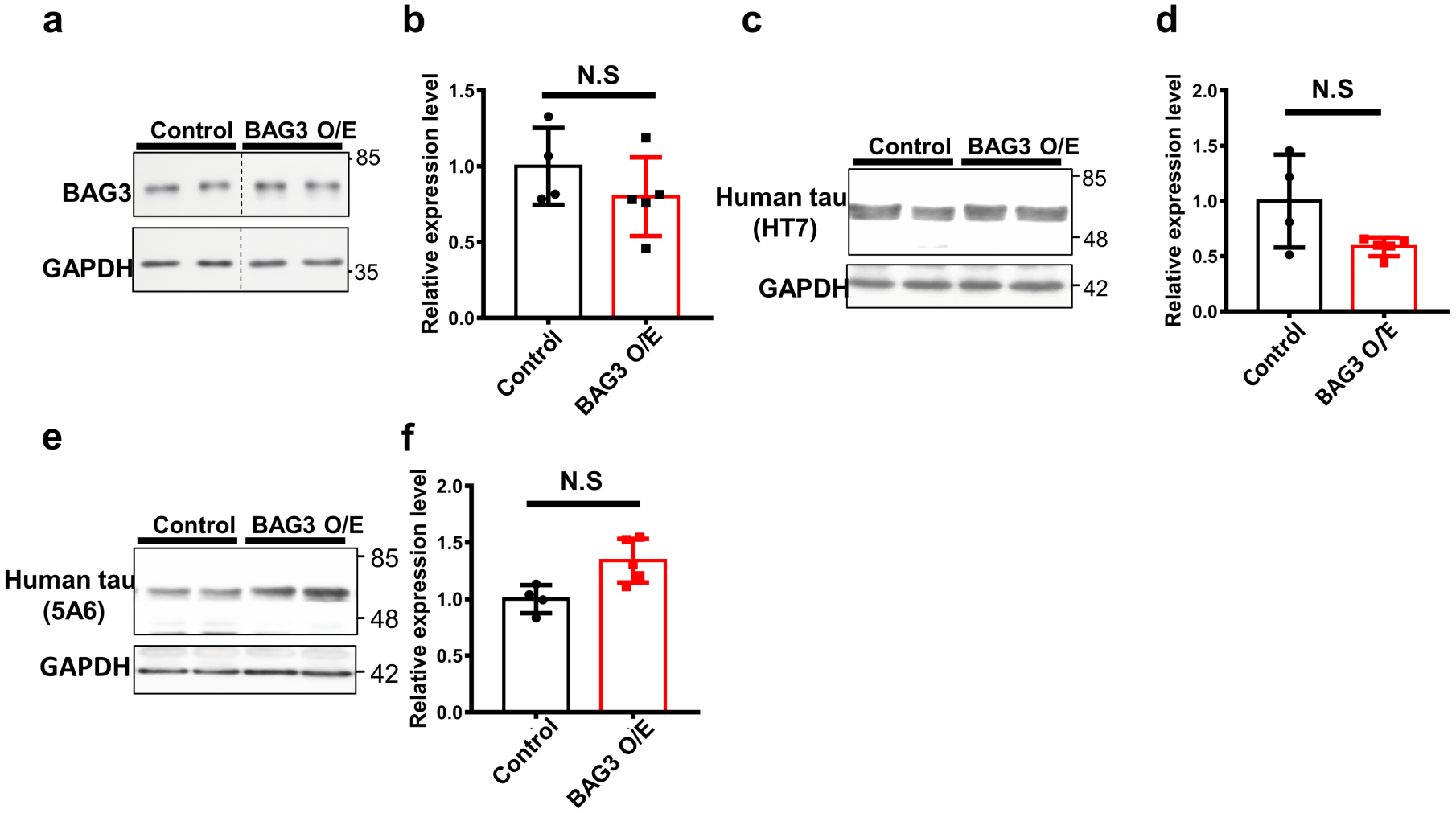

Fig s3. Overexpression of BAG3 in the hippocampus doesn't affect the tau levels in the cerebellum. Two-month-old P301S mice were intrahippocampal injected with AAV2/9-GFP as control or AAV2/9-GFP-BAG3-MYC as BAG3 overexpression (BAG3 O/E) and were collected at 6-month old. (a) Representative immunoblots of BAG3 for cerebellum lysate of control and BAG3 O/E brains. (b) The graph shows the quantitative analysis of BAG3 to GAPDH and relative to control. (c, e) Representative blot of total tau (HT5 and 5A6) for cerebellum lysates of control and BAG3 O/E brains. (d, f) The graphs show the quantitative analysis of tau to GAPDH and relative to control. N=4 for control, n=5 for BAG3 O/E. Data are shown as mean ± SEM. Statistical analysis was performed using the student t-test. NS, not significant.